ABSTRACT

LAWRENCE, JOSHUA FOOTE. Torque Converter Predictive Modeling Validation in a Post Transmission Parallel Hybrid Drive Train. (Under the direction of Dr. Eric Klang and Dr. Ewan Pritchard.)

In 2005, the first ever commercially available plug-in vehicle entered the transportation market in the form of a school bus. As a part of a collaborative effort between NC State University and Advanced Energy, an independent non-profit, 15 plug-in buses were manufactured and deployed to school districts across the country in hopes of increasing fuel economy and decreasing tail pipe emissions. However, the buses failed to perform up to the predicted modeling generated by ADVISOR. This sparked interest as to why. Follow up research, conducted at the Advanced Transportation Energy Center at North Carolina State University, suggested that due to the Plug in Hybrid Electric School Bus (PHESB) architecture, there was a much greater loss in the torque converter than the ADVISOR models predicted, more specifically in the overrunning regime. New predictive models were developed to account for the overrunning regime and when implemented into the modeling software, an energy loss over one drive cycle yielded a loss 19 times greater than that given by ADVISOR. These losses apply not only to PHESBs, but all aftermarket hybrid conversion vehicles that use the same architecture.

This thesis validates the mathematical models for the torque converter with in lab testing. An electric dynamometer test bed was built and a torque converter was mounted between the two motors. Experimental setup included disassembling a transmission from the PHESB and modifying its components to work within the test bed. An external fluid system was designed to replicate the fluid system internal to the transmission. Experimental testing took place over a range of speed

ratios that validated the predictive models for internal loss in the torque converter with an emphasis on the overrunning regime. These experimental tests have been completed and the results are presented.

Torque Converter Predictive Modeling Validation in a Post Transmission Parallel Hybrid Drive Train

by
Joshua Foote Lawrence

A thesis submitted to the Graduate Faculty of
North Carolina State University
In partial fulfillment of the
requirements for the degree of
Master of Science

Mechanical Engineering

Raleigh, North Carolina

2013

APPROVED BY:

_____	_____
Dr. Eric Klang Committee Chair	Dr. Srdjan Lukic
_____	_____
Dr. Jeffrey Eischen	Dr. Ewan Pritchard

Dedication

This work is dedicated to my parents. Without their unwavering support I would not be who or where I am today.

Biography

Joshua Foote Lawrence was born on June 16, 1987 in Wilmington, North Carolina to Jane and Richard Lawrence. He grew up and completed his grade school in Wilmington, where he learned to love anything outdoors. He always had a passion for math and science that drove him to pursue a Bachelor's Degree in Mechanical Engineering. During that time, he worked for a non-profit called Advanced Energy where he learned how he could apply his degree in a way that would make a positive impact on the environment. His involvement at Advanced Energy in the transportation sector fueled his interest in electric transportation. He received his Bachelor's Degree in Mechanical Engineering in 2010. He continued to follow his passion for alternative energy and electric transportation by pursing his Master's Degree under the direction of Dr. Ewan Pritchard and Dr. Eric Klang.

Acknowledgements

There are so many people who have helped me tremendously along the path to where I am today and for that I am forever grateful. First, I would like to thank Dr. Ewan Pritchard for planting the seed in my head about pursuing graduate school. His encouragement, guidance, friendship and shared passion are the reason I am a part of the FREEDM family.

I would like to thank Dr. Eric Klang for providing his support, guidance, and patience throughout the duration of my research. His positive outlook and attitude were always uplifting and provided the boosts needed to get through this effort.

I would like to thank Dr. Srdjan Lukic for guiding me throughout this process with his knowledge and expertise. I would have been lost without his help.

I would like to thank Dr. Iqbal Husain for helping me get over a lot of the speed bumps encountered during my research. His willingness to help and passion for sharing knowledge was inspirational.

I would like to thank Dr. Richard Johnson for going out of his way to provide his positive encouragement and expertise. His interest and passion in my research lit a new fire in me. His thirst for knowledge and thought provoking queries helped shape my thesis.

I would like to thank all of my family and friends for believing in me and providing unparalleled encouragement, support, and sometimes the necessary distraction to clear my head and gather my thoughts. This process truly could not have happened without them.

Lastly, but definitely not least, I would like to express my deepest gratitude to Lacy Dean. Without her none of this would have been possible.

Table of Contents

List of Tables

List of Figures

Nomenclature

Symbol	Description (Assumed value where applicable)	Units
α_{ie}	impeller entry angle in positive flow	rad
α_{ix}	impeller exit angle in positive flow	rad
α_{te}	turbine entry angle in positive flow	rad
α_{tx}	turbine exit angle in positive flow	rad
α_{se}	stator entry angle in positive flow	rad
α_{sx}	stator exit angle in positive flow	rad
$\alpha_{ié}$	impeller entry angle in negative flow	rad
$\alpha_{ix\acute{}}$	impeller exit angle in negative flow	rad
$\alpha_{té}$	turbine entry angle in negative flow	rad
$\alpha_{tx\acute{}}$	turbine exit angle in negative flow	rad
$\alpha_{sé}$	stator entry angle in negative flow	rad
$\alpha_{sx\acute{}}$	stator exit angle in negative flow	rad
τ_i	impeller torque (engine)	N-m
τ_s	stator torque	N-m
τ_t	turbine torque (transmission)	N-m
ω_i	impeller angular speed	rad/s
ω_t	turbine angular speed	rad/s

Symbol	Description (Assumed value where applicable)	Units
ω_s	stator angular speed	rad/s
A_{ie}	impeller entry area in positive flow	m^2
A_{ix}	impeller exit area in positive flow	m^2
A_{te}	turbine entry area in positive flow	m^2
A_{tx}	turbine exit area in positive flow	m^2
A_{se}	stator entry area in positive flow	m^2
A_{sx}	stator exit area in positive flow	m^2
$\acute{A}_{ie}$	impeller entry area in negative flow	m^2
$\acute{A}_{ix}$	impeller exit area in negative flow	m^2
$\acute{A}_{te}$	turbine entry area in negative flow	m^2
$\acute{A}_{tx}$	turbine exit area in negative flow	m^2
$\acute{A}_{se}$	stator entry area in negative flow	m^2
$\acute{A}_{sx}$	stator exit area in negative flow	m^2
C_f	friction coefficient (0.5)	-
C_p	Battery Capacity	A-h
k	Peukert Coefficient	-
ρ	transmission fluid density (Dextron, 844.3 kg/m^3)	kg/m^3
Q	torque converter secondary flow rate	m^3/s
r_{ie}	impeller entry radius in positive flow	m

Symbol	Description (Assumed value where applicable)	Units
r_{ix}	impeller exit radius in positive flow	m
r_{te}	turbine entry radius in positive flow	m
r_{tx}	turbine exit radius in positive flow	m
r_{se}	stator entry radius in positive flow	m
r_{sx}	stator exit radius in positive flow	m
$\acute{r}_{ie}$	impeller entry radius in negative flow	m
$\acute{r}_{ix}$	impeller exit radius in negative flow	m
$\acute{r}_{te}$	turbine entry radius in negative flow	m
$\acute{r}_{tx}$	turbine exit radius in negative flow	m
$\acute{r}_{se}$	stator entry radius in negative flow	m
$\acute{r}_{sx}$	stator exit radius in negative flow	m
SR	speed ratio	-
TR	torque ratio	-
$\dot{L}_{ix}$	angular momentum change leaving the impeller	kg-m^2/s^2
$\dot{L}_{tx}$	angular momentum change leaving the turbine	kg-m^2/s^2
$\dot{L}_{sx}$	angular momentum change leaving the stator	kg-m^2/s^2

Chapter 1

Introduction

As with any hybrid vehicle on the road today, their purpose is to reduce fuel consumption, increase overall efficiency and ultimately reduce greenhouse gas tail pipe emissions. With federal emission standards becoming increasingly strict, domestic vehicle manufacturers are turning to hybrid and electric vehicles to meet the new mandates. One niche that caught on early is the heavy duty market, more specifically school busses. This effort was driven by the work of Advanced Energy, a non-profit organization located in Raleigh North Carolina. *Performance Modeling of Hybrid and Plug-in Hybrid School Buses Using ADVISOR* by Pritchard details the increased efficiency and decreased tailpipe emissions of a variety of different school bus drive trains with both series and parallel hybrid architecture [1]. Pritchard's work at Advanced Energy eventually led to the development of the first ever commercially available plug-in hybrid electric vehicle. International Corporation teamed up with Enova Systems to build the plug-in hybrid electric school bus (PHESB). Enova Systems integrated an 80 kW electric motor hybrid drive system into the chassis of an International bus with the hopes of reducing overall fuel consumption. However, the overall reduction did not correlate with the anticipated results based on modeling using ADVISOR. In Advanced Energy's *Plug-in Hybrid Electric School Bus Project: 2010 Program Report* it was clear that the modified PHESBs were not performing as well as predicted [2].

1.1 PHESB System Loss Investigation

Because the PHESBs were not performing as expected, investigations took place into exactly why the efficiency was so low and more specifically what was the exact cause. Three different potential

causes were investigated: poor battery performance, engine braking creating a drag on the electric motor, and losses in the torque converter. A closer look indicated that because of the post transmission parallel hybrid architecture of the PHESB and lack of communication between the engine and hybrid systems there was excessive loss in the torque converter over the vehicle operating range [3].

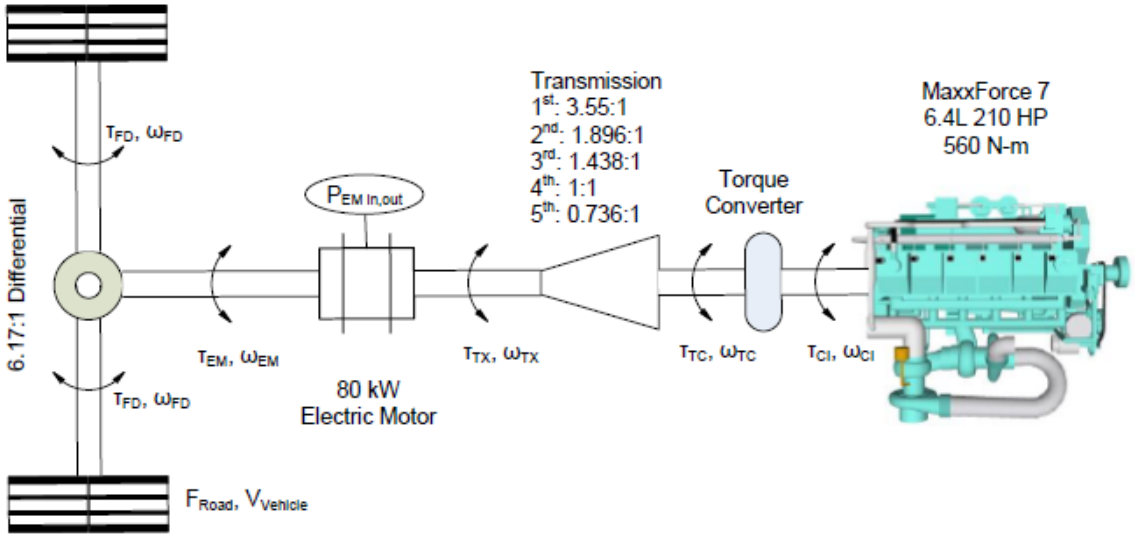

Figure 1-1: PHESB Drive Train Components [3]

Therefore, the majority of research focused on characterizing the torque converter losses.

1.2 Torque Converter Interactions in Drive Train

Torque converters are widely utilized in vehicles with automatic transmissions. Their purpose is transfer torque from the engine to the transmission and then the final drive. The torque converter is coupled to the engine's flywheel and spins at engine speed. The converter consists of three major parts: the impeller, the turbine and the stator. The impeller is a form of a pump, with vanes

attached to the housing that drives fluid into the vanes located on the turbine. The turbine rotates as fluid is transferred from one side of the converter to the other and is directly coupled to the transmission with the turbine output shaft. The stator rotates on a one way clutch and is located between the vanes of the impeller and the turbine. It is used to redirect fluid flow from the turbine to the impeller at low engine speeds and allows for torque multiplication. As the ratio of impeller speed and turbine speed approaches 1, the stator will free wheel and is no longer used for fluid redirection. Once the torque converter reaches a certain pressure, a lock up clutch is engaged and the coupling becomes rigid.

There are three different modes or regimes of torque converter operation [4]:

- Below coupling: Speed ratio (SR) from zero to approximately 0.9 where the stator is locked in place by the one-way clutch redirecting fluid.
- Above coupling: SR from 0.9-1. The coupling point has been reached and the stator is spinning freely with positive vortex flow.
- Overrunning: SR greater than 1. Stator is spinning freely, but now the vortex flow is negative.

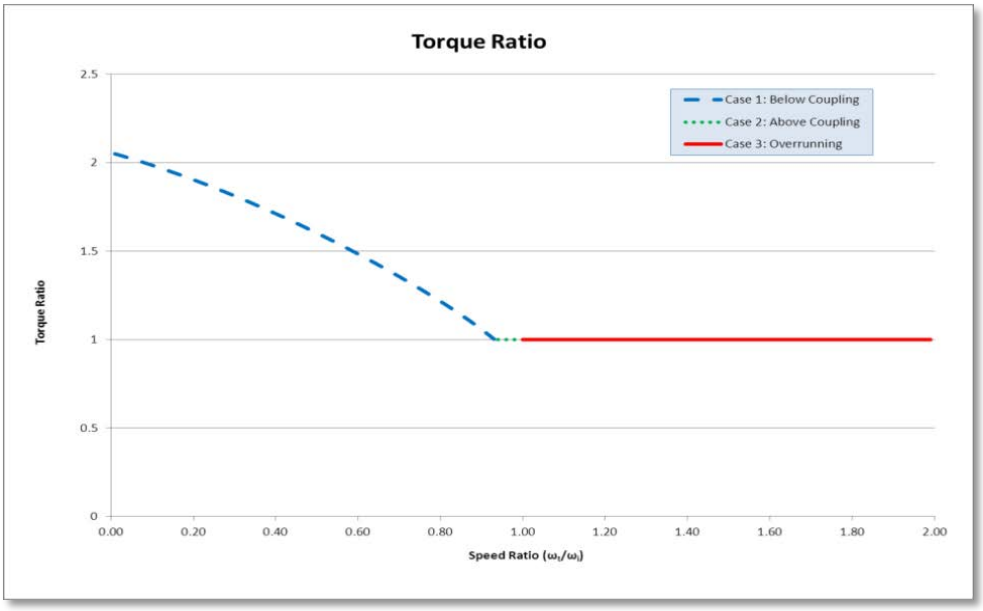

Figure 1-2: Torque Ratio vs. Speed Ratio [3]

Figure 1-2 illustrates these operating regions, comparing speed ratio and torque ratio. The mode of operation that is of most concern with the PHESB drive train is overrunning. This occurs when the transmission side of the torque converter (the turbine) has a higher angular velocity than the engine side (the impeller). Traditionally, research on torque converters has been limited to speed ratios below one. This can be attributed to the fact that in conventional internal combustion vehicles there was never a need to understand overrunning and its effect on vehicle performance. With two power plants driving the vehicle, one positioned after the transmission, it becomes imperative to understand how the torque converter works in both modes and how that ultimately affects overall vehicle performance. Further detailed description and investigation of the complex fluid flow occurring inside the torque converter is presented in Chapter 2.

Using data collected from PHESB operation, shown in Figure 1-3, it is clear that the areas of concern are when the motor speed is greater than the engine speed in 1st and 2nd gears. These low speed lower power demand situations occur when the electric motor is utilized to supplement the diesel engine. During these operation modes the converter is operating in the overrunning regime causing a system power loss, thus decreasing the overall efficiency of the system from heat losses in both the torque converter and engine.

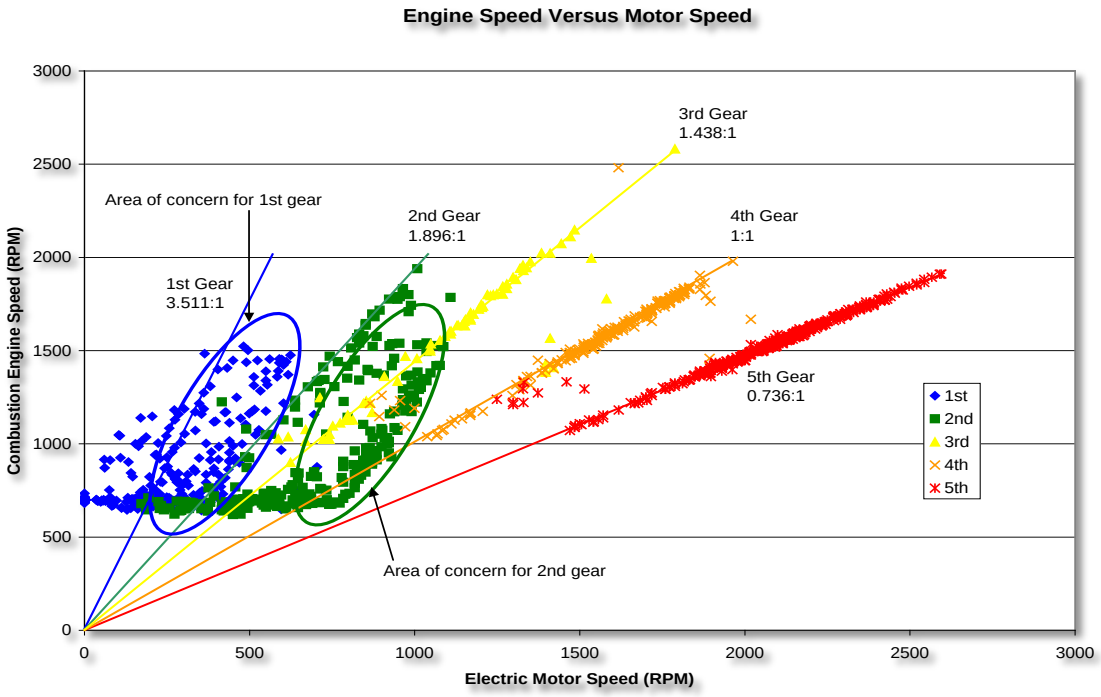

Figure 1-3: Combustion Electric Motor Speed vs. Combustion Engine Speed [3]

When the torque converter is overrunning, the internal fluid flow rate, Q, is reversed. This is an issue because it increases both friction and shock losses.

1.3 Computer Modeling

Most vehicle modeling systems including ADVISOR, a MATLAB/Simulink simulation tool developed by the National Renewable Energy Lab (NREL), which was used for Pritchard's study, utilize look up tables to account for the losses inside the torque converter. However, these losses are only defined in the operating ranges with a speed ratio less than one, when the impeller of the torque converter is spinning faster than the turbine. When the transmission spins faster than the engine, the look up tables used to estimate performance of the torque converter are reversed and do not account for the extra friction and shock losses occurring inside the torque converter in this regime, which is the main reason overrunning has not been a concern to both vehicle modeling software and vehicle production companies. In a conventional internal combustion engine (ICE) vehicle this situation only occurs when slowing down or traveling downhill. The addition of the electric motor increases the amount of time the torque converter is operating in the overrunning regime. Pritchard created predictive equations for this specific case to implement into ADVISOR that account for the additional losses occurring inside the torque converter for a post transmission parallel hybrid drive train. The torque converter was modeled mathematically, and when this characterization was added to the existing ADVISOR model for the same drive train and drive cycle, the results varied drastically. When considering losses from torque converter overrunning, shown by the various jumps, the energy loss over one drive cycle was 683 W-h compared to 36 W-h predicted by ADVISOR, as seen in Figure 1-4.

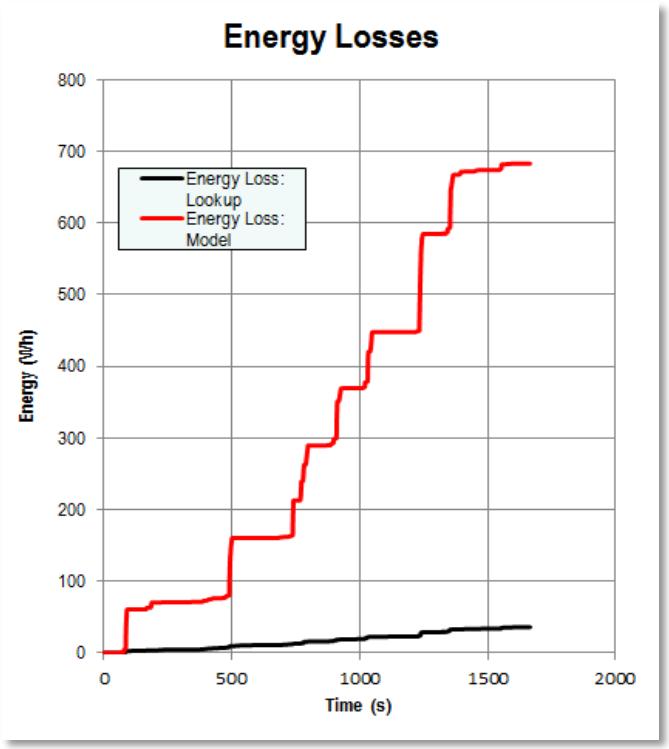

Figure 1-4: Energy Losses Using Torque Converter Overrunning [3]

Torque converter losses were calculated through a series of complex fluid flow calculations. Taking into consideration the internal fluid flow and the losses in each of the three components of the torque converter allowed for a more accurate ADVISOR model to predict vehicle performance. It also clearly indicated that ADVISOR did not take into consideration the overrunning operating range of the torque converter. The purpose of this study is to validate these results with in lab testing using an electric dynamometer.

1.4 Allison 2500 PTS Transmission

The hybrid electric school buses use a V-8 MAXXFORCE 7 turbo-diesel engine [5] coupled to an Allison 2500 PTS Series transmission, which uses a model TC-210 Torque converter.

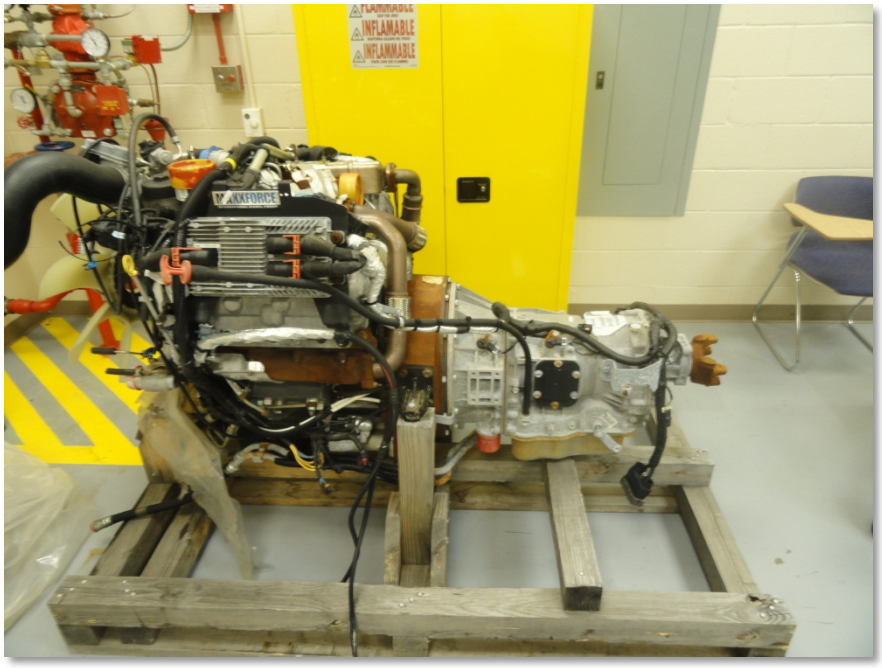

Figure 1-5: MAXXFORCE 7 Engine coupled to an Allison 2500PTS Transmission

For testing purposes, the transmission was decoupled from the engine and completely disassembled. Because of the complexity of the transmission this was imperative to ensure proper knowledge of the how the transmission and all components operate to achieve proper vehicle performance. Additionally, the transmission was taken apart to remove any components needed to implement into the test bed to create a system as close as possible to real world.

Chapter 2

Torque Converter Operation

2.1 Two-Stage Torque Converter

To fully understand the problem at hand, it is important to understand the complexity of the torque converter operation. The torque converter, a type of hydrodynamic coupling, was initially developed in 1902 by Dr. Foettinger for ship propulsion. He developed the first ever hydraulic transmission to drive the screw propeller on a ship in place of the traditional mechanical transmission. He created a case that consisted of an impeller pump and turbine, which drove the prop shaft. His invention yielded efficiency results of up to 97%, a drastic improvement from the traditional mechanical transmission [6] . At this early stage, the torque converter consisted of two stages and was referred to as a fluid coupling or two-stage torque converter. This allowed for the engine to run without transmitting torque to the transmission. Figure 2-1 shows the two components of a torque coupling, the impeller and the turbine.

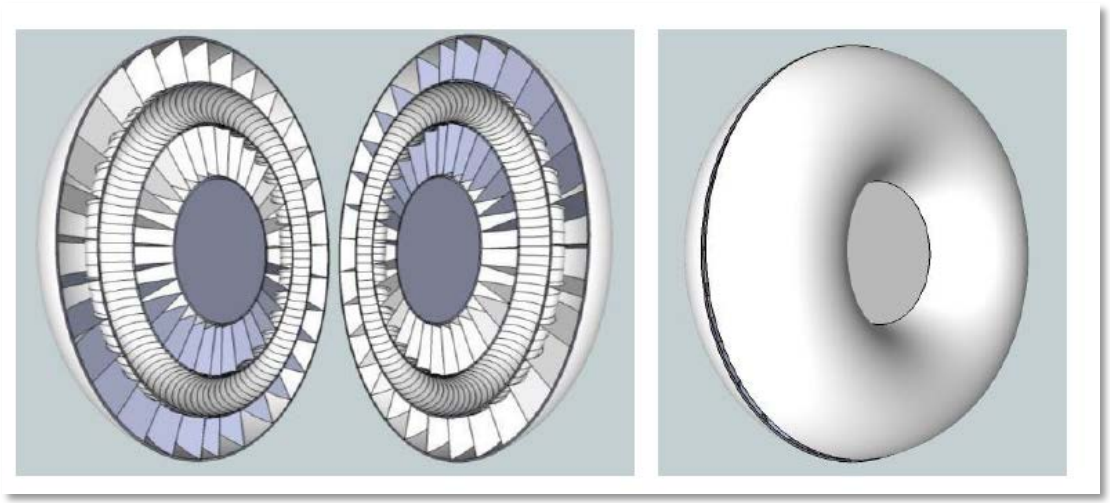

Figure 2-1: Two-Stage Torque Converter [3]

As the transportation sector grew, so did the use of torque converters. In the United States became very popular in the early 1930's. In addition to its durability, simplicity of construction, and smooth operation, the two-stage torque converter also provided torsional damping at all operating speeds and reduced the shock placed on the driveline [7]. However, the main issue with the two-stage torque coupling was that at low speed ratios, minimal torque was being transferred from the engine to the transmission causing poor vehicle performance and reduced drive train efficiency. This was because the turbine quickly reached the speed of the impeller, a stage known as coupling, and limited the torque transfer to a ratio less than one. Two important ratios to consider when characterizing a torque converter are the speed ratio (SR) and torque ratio (TR). Speed ratio is defined as the angular velocity of the turbine (ω_t) over the angular velocity of the impeller, coupled to the engine (ω_i). This is shown in Equation 2.1.

$$SR = \frac{\omega_t}{\omega_i} \tag{1.1}$$

Torque ratio (TR) is defined as turbine torque (τ_t) over impeller torque (τ_i) as seen in Equation 2.2.

$$TR = \frac{\tau_t}{\tau_i} \tag{1.2}$$

The two types of flow that occur inside a hydrodynamic coupling, rotary and vortex, are dictated by the shape and design of the blades on both the impeller and the turbine. In a two-stage design, the rotary flow creates a centrifugal force by pushing the fluid to the outside of the torque converter increasing the speed of both sides. The vortex flow is caused by a differential speed between the impeller and the turbine utilizing the blade angles to transfer fluid from the impeller to the turbine

and back. However, as the two sides approach the same speed, vortex flow is essentially eliminated while rotary flow takes over. The lag between engine torque to the final drive and inefficiency of the two-stage torque converter led to the development of the three-stage torque converter [8].

2.2 Three-Stage Torque Converter

In addition to the impeller and turbine, the three-stage hydrodynamic torque converter uses a reactor or stator between the impeller and turbine to redirect fluid flow from the center of the turbine back to the impeller. The addition of the stator effectively increases the vortex flow and with it the output torque going to the transmission.

As described earlier, two types of flow occur in the torque converter during operation, rotary flow and vortex flow. This is illustrated in Figure 2-2, where the rotary flow is marked by the blue path and vortex flow, Q, is marked by the red path.

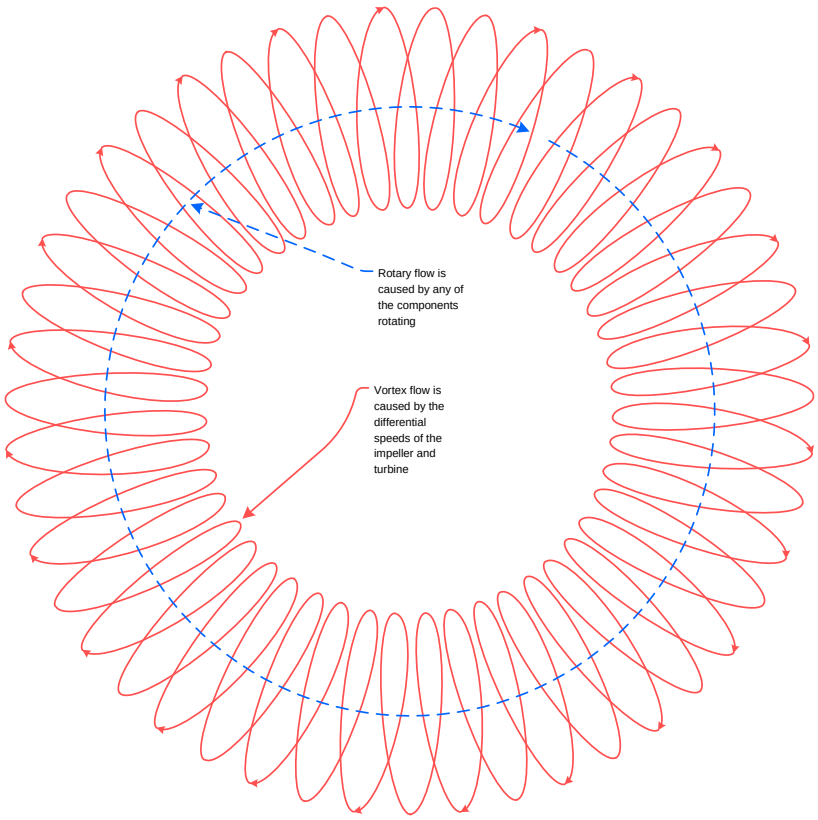

Figure 2-2: Internal Torque Converter Fluid Flow Path

2.3 Lock-up Clutch Operation

As the speed ratio of the torque converter approaches one, the vortex flow is reduced and approaches zero. The main flow at this point is the rotary flow as the centrifugal force pushes the fluid to the outside of the torque converter. Although this is a very efficient operating range, there will still be internal fluid losses. This sparked the implementation of a lock-up clutch that can be engaged to convert the fluid coupling into a rigid coupling. The operation of the lock-up clutch is vehicle dependent; however, it generally takes place when the vehicle is in 3rd gear or higher and travelling faster than approximately 35 mph. When coupled to the MAXXFORCE 7 diesel engine, the

Allison transmission engages the lock-up clutch in the TC-210 torque converter at speeds greater than approximately 37 mph or in 3rd gear or higher. The clutch plate engagement is controlled by fluid pressure. When the TCM receives a signal that either of those conditions is met, it actuates the torque converter clutch solenoid. This redirects the transmission fluid path causing the automatic transmission fluid (ATF) to enter in the opposite direction and pushes the clutch plate onto the torque converter housing. The clutch lock-up occurs at the above coupling point for the torque converter where torque multiplication no longer takes place. Once the vehicle starts to coast or slow down, the clutch disengages and allows for torque converter overrunning [9].

2.4 Two-Stage Torque Converter Fluid Modeling

Although the design of the torque converter is fairly simple, characterizing the internal flow is extremely complicated. The physical phenomenon that occurs inside the torque converter is dependent on very complicated fluid to blade interactions and its relationship to the fluid angular momentum [10]. There have been many studies published on torque converter operation for predictive analysis and modeling, however, very little investigation into torque converter operation at speed ratios greater than one. *Dynamic Models for Torque Converter Equipped Vehicles* by Kotwicki looks at a simplified model of a torque converter based on the principle that the time rate of change of angular momentum in the transmission fluid moving through a stationary or rotating element equals the torque applied to that element [11]. The rotational angular momentum of the moving fluid in the vortex flow inside the torque converter is transferred from the blades of the impeller to the turbine blades, which yields a torque output. This basic theory and principle is also supported in *Introduction to Fluid Mechanics* by Fox and McDonald [12]. To analyze this

theoretically, a simplified model is assumed using a two-stage torque converter with flat blades and constant speed. This is shown in Figure 2-3.

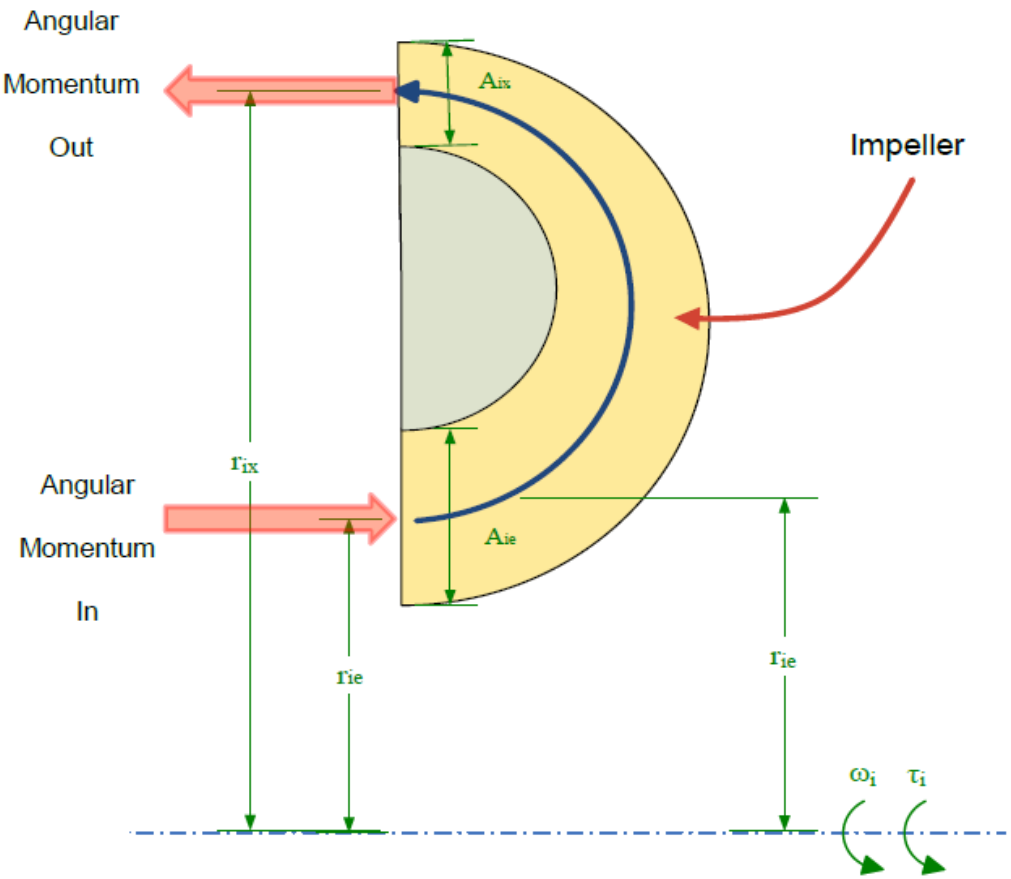

Figure 2-3: Simplified Torque Converter Model [3]

When the impeller begins to rotate an applied torque is generated that induces a volumetric flow rate, Q, through the impeller and turbine. The impeller exit angular momentum flow rate is defined as:

$$\dot{L}_{ix} = \rho Q r_{ix}{}^{2} \omega_i \tag{2.1}$$

The turbine exit angular momentum is found using the same calculation method, and is:

$$\dot{L}_{tx} = \rho Q r_{tx}{}^{2} \omega_t \tag{2.2}$$

As previously stated, the torque must equal the time rate change of the angular momentum of the fluid passing through the two elements. Turbine torque is shown in Equation 2.3.

$$\tau_t = \dot{L}_{tx} - \dot{L}_{ix} = \rho Q (r_{tx}^2 \omega_t - r_{ix}^2 \omega_i) \tag{2.3}$$

Similarly, the impeller torque is defined as:

$$\tau_i = -\tau_t = \dot{L}_{ix} - \dot{L}_{tx} = \rho Q (r_{ix}^2 \omega_i - r_{tx}^2 \omega_t) \tag{2.4}$$

The impeller and turbine torques are equal in magnitude in this simplified analysis, but in opposite directions. The relationship of power to torque is multiplied by angular velocity to find the turbine and pump power in Equations 2.5 and 2.6, respectively.

$$P_t = \rho Q \omega_t (r_{tx}^2 \omega_t - r_{ix}^2 \omega_i) \tag{2.5}$$

$$P_i = \rho Q \omega_i (r_{ix}^2 \omega_i - r_{tx}^2 \omega_t) \tag{2.6}$$

To find the losses in this simplified fluid coupling system, or rather the rate at which energy is dissipated, the pump and turbine power are combined.

$$P_i + P_t = \rho Q \omega_i (r_{ix}^2 \omega_i - r_{tx}^2 \omega_t) + \rho Q \omega_t (r_{tx}^2 \omega_t - r_{ix}^2 \omega_i) \tag{2.7}$$

This is can be rewritten as:

$$P_i + P_t = \rho Q(r_{ix}^2\omega_i^2 - r_{tx}^2\omega_t\omega_i + r_{tx}^2\omega_t^2 - r_{ix}^2\omega_t\omega_i) \tag{2.8}$$

This power loss can also be represented by pressure by dividing out the volumetric flow rate.

$$\Delta p_i + \Delta p_t = \rho(r_{ix}^2\omega_i^2 - r_{tx}^2\omega_t\omega_i + r_{tx}^2\omega_t^2 - r_{ix}^2\omega_t\omega_i) \tag{2.9}$$

Now that the losses are in terms of pressure, a relationship is developed to account for the total system losses by two sources, friction and shock loss. Fluid friction is proportional to the square of the volumetric flow rate:

$$\Delta p_f = \frac{1}{2}\rho C_f Q^2 \tag{2.10}$$

Shock losses are caused by the sudden velocity change in the fluid as it hits the blades of the impeller and pump. This is defined as:

$$\Delta p_{sl} = \frac{1}{2}\rho r_{ix}^2(\omega_i - \omega_t)^2 - \frac{1}{2}\rho r_{tx}^2(\omega_t - \omega_i)^2 \tag{2.11}$$

In steady state conditions, the complete fluid energy of the system must equate to zero. Therefore, a relationship between power losses, represented as pressure, and the two source losses can be developed.

$$\rho(r_{ix}^2\omega_i^2 - r_{tx}^2\omega_t\omega_i + r_{tx}^2\omega_t^2 - r_{ix}^2\omega_t\omega_i) = \frac{1}{2}\rho C_f Q^2 + \frac{1}{2}\rho(r_{ix}^2 + r_{tx}^2)(\omega_i - \omega_t)^2 \tag{2.12}$$

Solving equation 3.12 for Q yields:

$$Q = \left(\frac{r_{ix}^2 - r_{tx}^2}{C_f} \right)^{1/2} (\omega_i^2 - \omega_t^2)^{1/2} \tag{2.13}$$

Substituting this equation for volumetric flow rate back into equations 2.3 and 2.4 yields a relationship between angular velocities and torques. This derivation allows you to arrive at Q using known variables and use that to find torque. Impeller and turbine torques are equal in magnitude and opposite in direction. Q is not easily measured experimentally but is a useful modeling variable. This relationship is used in the development of the Kotwicki Study and is the basis for Pritchard's predictive equation development of energy loss in the PHESB [3,11]. However, this relationship gets extremely complex when taking into consideration the addition of the stator and the blade angles as is shown in Kotwicki's study and *Torque Converter as a Vibration Damper and Its Transient Characteristics* by Ishihara and Emori [13]. This more complex derivation is shown in the following section.

2.5 Three-Stage Torque Converter Modeling

Using the same relationship of angular momentum and torque established in Section 2.4, the three regimes of torque converter operation can be modeled in terms of torque and speed for a three-stage torque converter. This evaluation does take into consideration both the stator and the entrance and exit angles of all three torque converter components as shown in Figure 2-4.

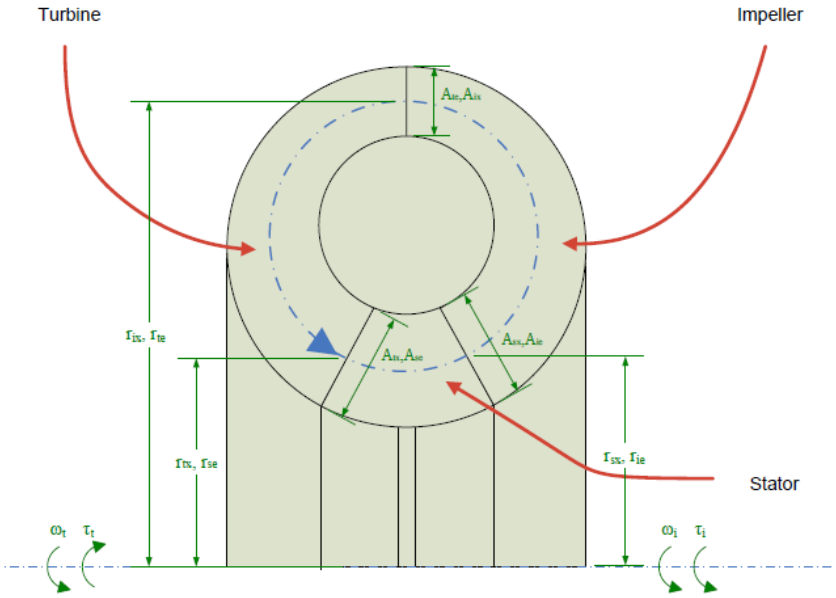

Figure 2-4: Regime 1 and 2 Geometry [3]

2.5.1 Below Coupling Regime

Using the relationships developed in section 2.4, Pritchard developed a quadratic equation that can be solved for Q [3]:

$$A_1 Q^2 + B_1 Q + C_1 = 0 \tag{2.14}$$

Where,

$$A_1 = \frac{1}{2}\rho\left[\left(\frac{\tan(\alpha_{ix})}{A_{ix}} - \frac{\tan(\alpha_{te})}{A_{te}}\right)^2 + \left(\frac{\tan(\alpha_{tx})}{A_{tx}} - \frac{\tan(\alpha_{se})}{A_{se}}\right)^2 + \left(\frac{\tan(\alpha_{sx})}{A_{sx}} - \frac{\tan(\alpha_{ie})}{A_{ie}}\right)^2 + cf\right] \tag{2.15}$$

$$B_1 = \rho\omega_t\left(\frac{r_{te}\tan\alpha_{te}}{A_{te}} - \frac{r_{tx}\tan\alpha_{se}}{A_{se}}\right) - \rho\omega_i\left(\frac{r_{ix}\tan\alpha_{te}}{A_{te}} - \frac{r_{ie}\tan\alpha_{ie}}{A_{ie}}\right) \tag{2.16}$$

$$C_1 = \frac{1}{2}\rho\left((r_{ix}^2 - r_{ie}^2)\omega_i^2 + (r_{tx}^2 - r_{te}^2)\omega_t^2\right) \tag{2.17}$$

This relationship established by Pritchard for the below coupling regime agrees with the study *Bond Graph Modeling and Computer Simulation of Automotive Torque Converters* by Hrovat and Tobler if steady state conditions are assumed [14]. Kotwicki's model also agrees, however, it assumes equal radii and areas. Therefore the above equations developed by Pritchard for the below coupling regime provide a more general analysis than those developed by Kotwicki and Hrovat and Tobler.

2.5.2 Above Coupling Regime

The above coupling regime is an operational mode where the TR is between approximately 0.9-1. In this regime the reactionary torque acting on the stator must be equal to or less than zero and the stator will begin to freewheel once a negative torque is applied to it. The torque converter will then begin to operate as a two-stage torque converter with an extra internal element that must be accounted for. Again, Pritchard developed this relationship yielding a result of a simple quadratic formula seen in equation 2.14. The coefficients in this regime are:

$$A_2 = \frac{1}{2}\rho\left[\begin{array}{l}\left(\frac{\tan(\alpha_{ix})}{A_{ix}} - \frac{\tan(\alpha_{te})}{A_{te}}\right)^2 + \left(\frac{\tan(\alpha_{sx})}{A_{sx}} - \frac{\tan(\alpha_{se})}{A_{se}}\right)^2 + \\ \left(\frac{\tan(\alpha_{ie})}{A_{ie}} - \frac{\tan(\alpha_{tx})}{A_{tx}}\right)^2 + cf\end{array}\right] \tag{2.18}$$

$$B_2 = \rho\omega_t\left(\frac{r_{te}\tan\alpha_{te}}{A_{te}} - \frac{r_{ie}\tan\alpha_{ie}}{A_{ie}}\right) - \rho\omega_i\left(\frac{r_{te}\tan\alpha_{te}}{A_{te}} - \frac{r_{ie}\tan\alpha_{ie}}{A_{ie}}\right) \tag{2.19}$$

$$C_2 = \frac{1}{2}\rho\left((r_{ix}^2 - r_{ie}^2)\omega_i^2 + (r_{tx}^2 - r_{te}^2)\omega_t^2\right) \tag{2.20}$$

Once again, this relationship agrees with those found by Kotwicki and Hrovat and Tobler. The relationships developed characterize all operating modes up to a SR of 1 [11,14]. However, neither Kotwicki or Hrovat and Tobler developed modeling equations for SR greater than 1, or the overrunning regime. Pritchard developed a new set of equations for this regime, which are provided in the next section.

2.5.3 Overrunning Regime

Using a similar derivation as above, Pritchard developed a relationship between volumetric flow rate, angular velocity and torque. It is important to note the new entrance and exit values that were used, shown in Figure 2-5.

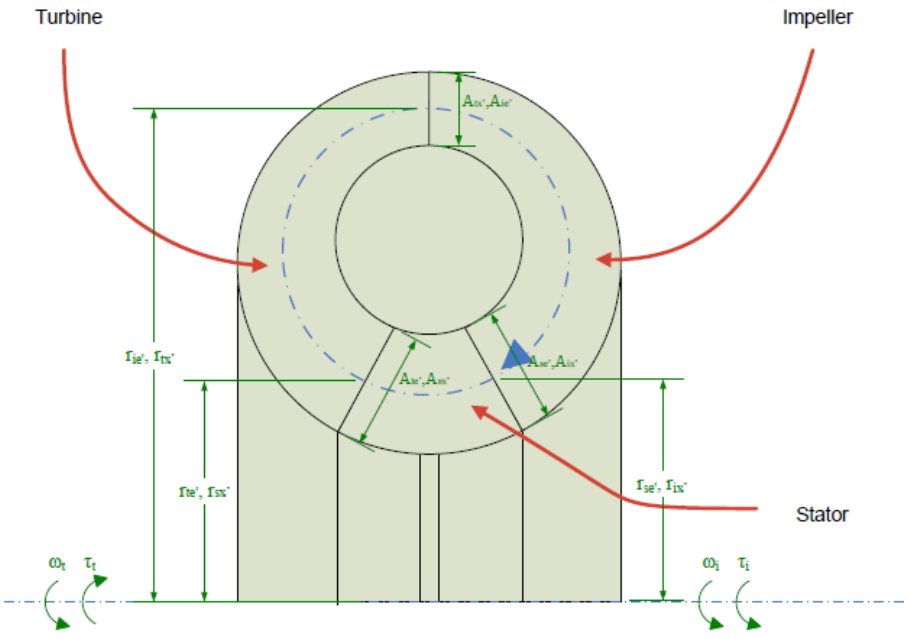

Figure 2-5: Regime 3 Geometry [3]

In the overrunning regime, the unit behaves as a two-stage torque converter with a torque ratio of one. However, the vortex flow rate, Q, will be negative, or rotating in the opposite direction. This means that not only will the entrance and exit values switch but also the side of the blade that the fluid first approaches will change. Hrovat and Tobler's study simply invert the blade angles and do not account for the side of the blade that the fluid first approaches [3]. The same approach is used as in the previous two regimes and the two-stage torque converter yielding a simple quadratic equation 2.14. Pritchard takes into consideration not only the change in blade geometry, but also the side of the blade that the fluid first hits and yields coefficients of:

$$A_3 = \frac{1}{2}\rho\left(\frac{\tan(\alpha_{ix})}{A_{ix}} - \frac{\tan(\alpha_{se})}{A_{se}} - \frac{\left(\frac{r_{ix}\tan(\alpha_{ix})}{A_{ix}} - \frac{r_{sx}\tan(\alpha_{sx})}{A_{sx}}\right)r_{se}}{r_{sx}^2}\right)^2$$
$$+\frac{1}{2}\rho\left(\frac{\tan(\alpha_{tx})}{A_{tx}} - \frac{\tan(\alpha_{ie})}{A_{ie}}\right)^2 \qquad (2.21)$$
$$+\frac{1}{2}\rho\left(\frac{\tan(\alpha_{sx})}{A_{sx}} - \frac{\tan(\alpha_{te})}{A_{te}} + \frac{\frac{r_{ix}\tan(\alpha_{ix})}{A_{ix}} - \frac{r_{sx}\tan(\alpha_{sx})}{A_{sx}}}{r_{sx}}\right)^2 + \frac{1}{2}\rho cf$$

$$
\begin{aligned}
B_3 &= \rho(\omega_t r_{tx} - \omega_i r_{ie})\left(\frac{\tan(\alpha_{tx})}{A_{tx}} - \frac{\tan(\alpha_{ie})}{A_{ie}}\right) - \rho\left(\frac{r_{tx}\tan(\alpha_{tx})}{A_{tx}} - \frac{r_{ix}\tan(\alpha_{ix})}{A_{ix}}\right)\omega_t \\
&+ \rho\left(\frac{\omega_i r_{ix}^2}{r_{sx}} - \omega_t r_{te}\right)\left(\frac{\tan(\alpha_{sx})}{A_{sx}} - \frac{\tan(\alpha_{te})}{A_{te}} + \frac{\frac{r_{ix}\tan(\alpha_{ix})}{A_{ix}} - \frac{r_{sx}\tan(\alpha_{sx})}{A_{sx}}}{r_{sx}}\right) \\
&+ \rho\left(\omega_i r_{ix} - \frac{\omega_i r_{ix}^2 r_{se}}{r_{sx}^2}\right)\left(\frac{\tan(\alpha_{ix})}{A_{ix}} - \frac{\tan(\alpha_{se})}{A_{se}} - \frac{\frac{r_{ix}\tan(\alpha_{ix})}{A_{ix}} - \frac{r_{sx}\tan(\alpha_{sx})}{A_{sx}} r_{se}}{r_{sx}^2}\right) \\
&+ \rho\left(\frac{r_{ix}\tan(\alpha_{ix})}{A_{ix}} - \frac{r_{tx}\tan(\alpha_{tx})}{A_{tx}}\right)\omega_i
\end{aligned}
\tag{2.22}
$$

$$
\begin{aligned}
C_3 &= \frac{1}{2}\rho(\omega_t r_{tx} - \omega_i r_{ie})^2 + \frac{1}{2}\rho\left(\frac{\omega_i r_{ix}^2}{r_{sx}} - \omega_t r_{te}\right)^2 + \frac{1}{2}\rho\left(\omega_i r_{ix} - \frac{\omega_i r_{ix}^2 r_{se}}{r_{sx}^2}\right)^2 \\
&- \rho(\omega_t r_{tx}^2 - \omega_i r_{ix}^2)\omega_t + \rho(\omega_i r_{ix}^2 - \omega_t r_{tx}^2)\omega_i
\end{aligned}
\tag{2.23}
$$

Pritchard developed this relationship and uses the following known variable values specific to the TC-210 torque converter found in the Allison 2500 PTS transmission, shown in Table 2-1. These predictive equations were applied to ADVISOR to account for energy loss when SR is greater than one.

Table 2-1: TC-210 Torque Converter Blade Angles [3]

Variable	Value	Variable	Value	Variable	Value
α_{ie}	0°	r_{ie}	0.0778 m	A_{ie}	0.019 m^2
α_{ix}	38°	r_{ix}	0.1365 m	A_{ix}	0.022 m^2
α_{te}	45°	r_{te}	0.1365 m	A_{te}	0.022 m^2
α_{tx}	-45°	r_{tx}	0.0778 m	A_{tx}	0.019 m^2
α_{se}	43°	r_{se}	0.0778 m	A_{se}	0.019 m^2
α_{sx}	75°	r_{sx}	0.0778 m	A_{sx}	0.019 m^2
$\acute{\alpha}_{ie}$	38°	$\acute{r}_{ie}$	0.1365 m	$\acute{A}_{ie}$	0.022 m^2
$\acute{\alpha}_{ix}$	0°	$\acute{r}_{ix}$	0.0778 m	$\acute{A}_{ix}$	0.019 m^2
$\acute{\alpha}_{te}$	-45°	$\acute{r}_{te}$	0.0778 m	$\acute{A}_{te}$	0.019 m^2
$\acute{\alpha}_{tx}$	45°	$\acute{r}_{tx}$	0.1365 m	$\acute{A}_{tx}$	0.022 m^2
$\acute{\alpha}_{se}$	75°	$\acute{r}_{se}$	0.0778 m	$\acute{A}_{se}$	0.019 m^2
$\acute{\alpha}_{sx}$	10°	$\acute{r}_{sx}$	0.0778 m	$\acute{A}_{sx}$	0.019 m^2

Chapter 3

Electric Vehicle Test Bed

3.1 Introduction

In order for testing to occur, a test bed needed to be fabricated that could simulate the engine and electric motor of the hybrid drive train and its interaction with the torque converter. The chassis of the test bed was first developed in the solid modeling program, SolidWorks, as seen in Figure 3-1.

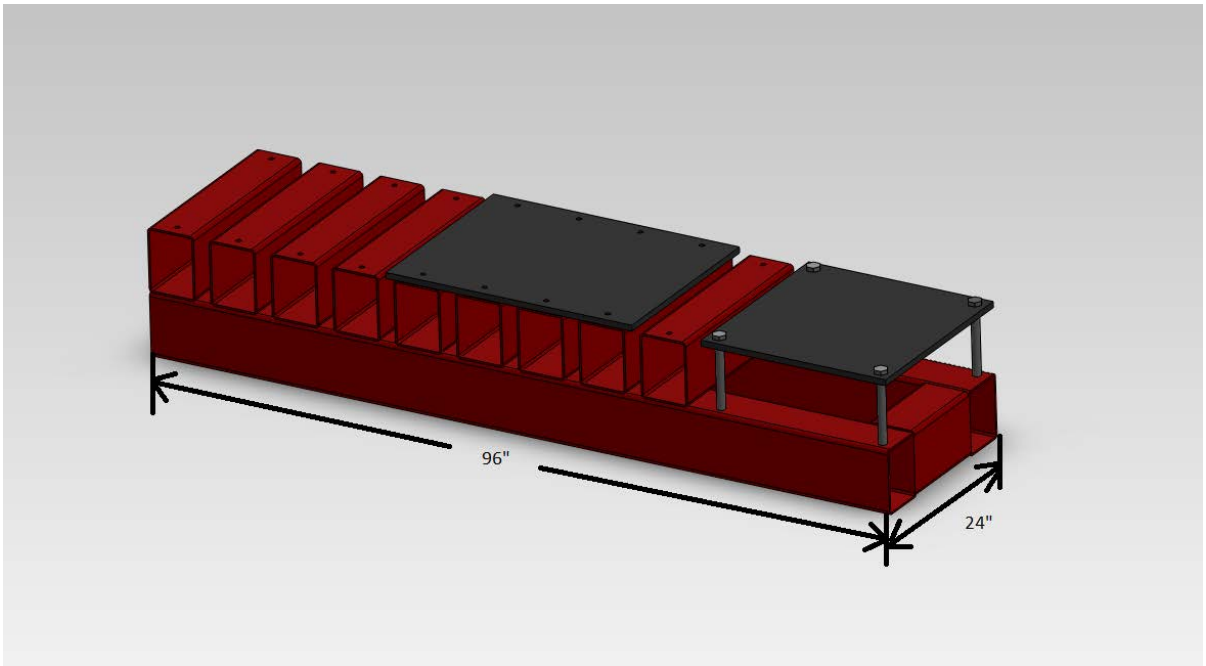

Figure 3-1: Electric Vehicle Test bed Chassis

This was used for mounting of both electric motors and eventually the torque converter mounting system.

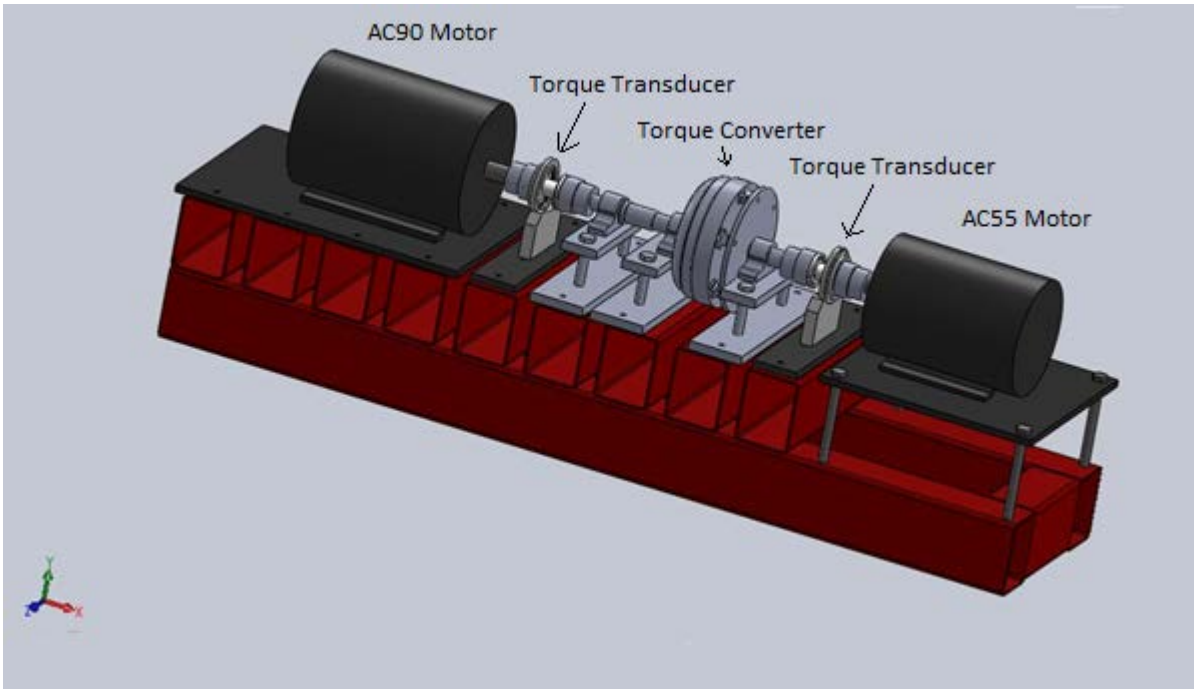

Figure 3-2: EV Test Bed Solid Model with Torque Converter Mounting System

Figure 3-2 shows the final solid model with all components mounted onto the test bed chassis. The test bed was designed to fit a wide variety of electric motors as well as additional drive train components. The mounting platform on the right hand side is fully adjustable to accommodate varying motor sizes.

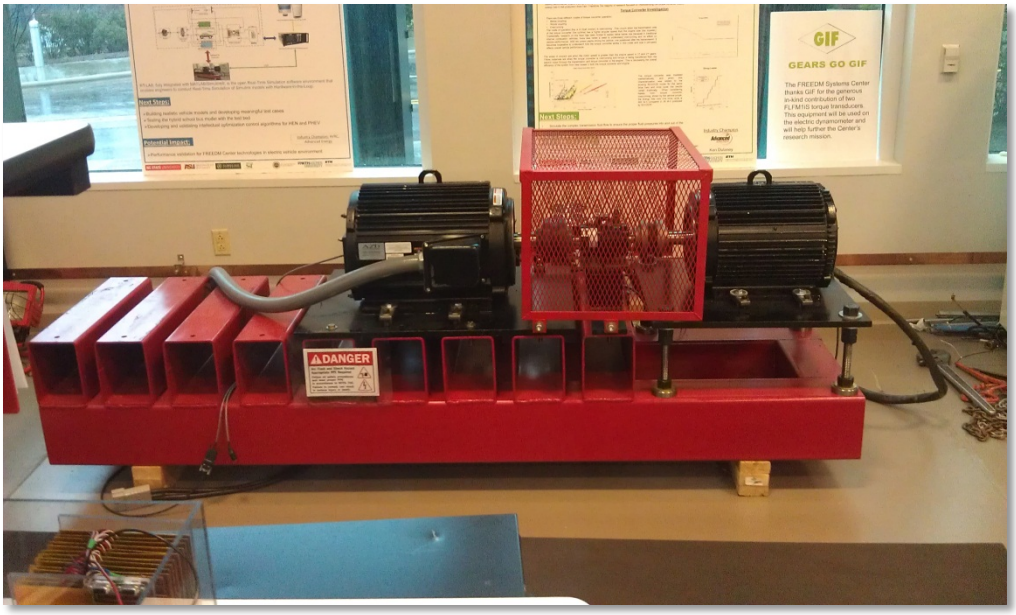

Figure 3-3: Fabricated EV Test Bed

Figure 3-3 shows the fabricated test bed before the torque converter mounting system was implemented.

3.2 Torque Converter Mount

The torque converter mount was fully adjustable allowing for easy alignment between the two electric motors. The stator shaft was fixed to the test bed to ensure it did not spin. It was also modified to allow for proper fluid flow into and out of the torque converter. The turbine shaft was modified to fit into a pillow block bearing and couple to the motor. In the PHESB, the torque converter bolts to the flywheel of the engine. A steel disc was fabricated with a shaft welded to its center to allow for coupling the torque converter directly to an electric motor. The EV test bed with the torque converter mounted is shown in Figure 3-4.

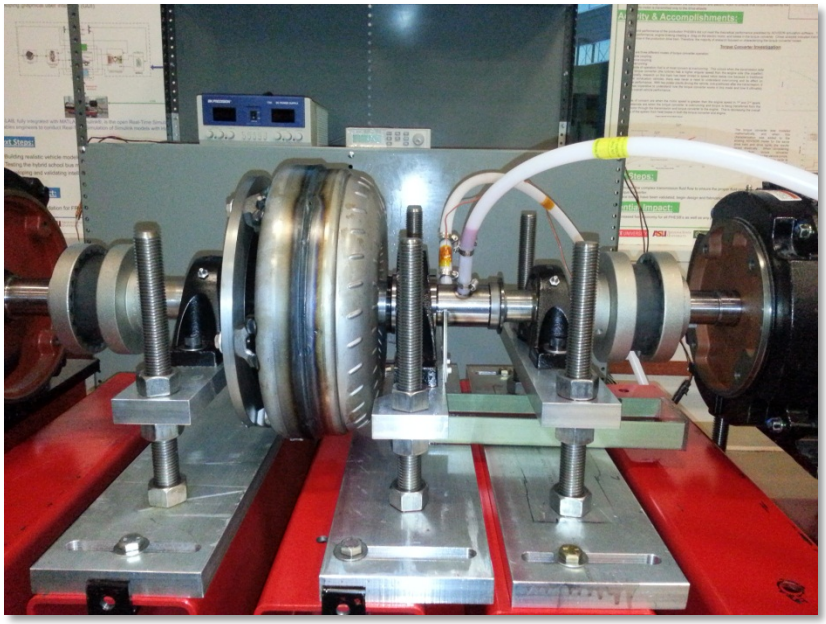

Figure 3-4: EV Test Bed With Torque Converter Mount

3.3 EV Test Bed Hardware

The test bed consists of two three-phase AC induction motors made by Azure Dynamics. The motor specifications are shown in Table 3-1 and Table 3-2 below.

Table 3-1: Azure Dynamics AC90 Motor Specifications

AC90 Motor Specifications		
Peak Torque	Nm	665
Continuous Torque at Nominal Speed	Nm	330
Nominal Speed	Rpm	1350
Maximum Mechanical Speed	Rpm	5000
Maximum Current	A rms	414
Continuous Shaft Power (at 312V DC)	kW	50
Peak Efficiency	%	94
Peak Shaft Power (at 312V DC)	kW	97

Table 3-2: Azure Dynamics AC55 Motor Specifications

AC55 Motor Specifications		
Peak Torque	Nm	280
Continuous Torque at Nominal Speed	Nm	140
Nominal Speed	Rpm	2000
Maximum Mechanical Speed	Rpm	8000
Maximum Current	A rms	250
Continuous Shaft Power (at 312V DC)	kW	25
Peak Efficiency	%	87
Peak Shaft Power (at 312V DC)	kW	59

The AC90 and AC55 motors are controlled by the DMOC645 and DMOC445 controllers, respectively.

Each motor drive requires a 12V dc power supply for internal circuitry.

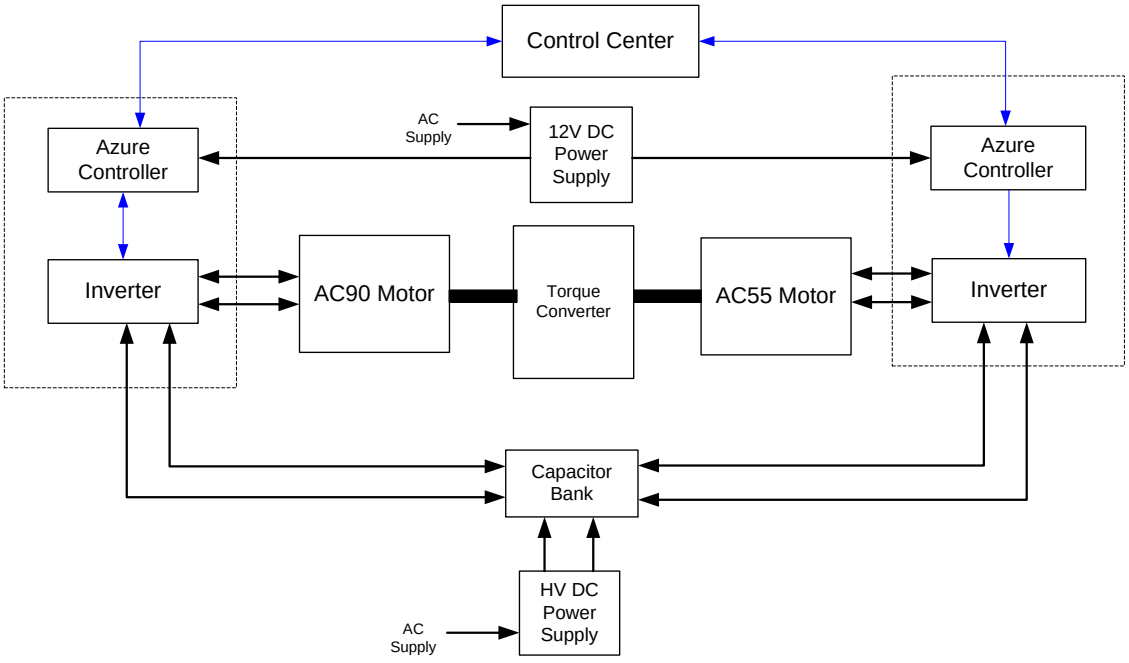

Figure 3-5: Hardware Block Diagram

The control center is an OPAL-RT hardware-in-the-loop system. It allows for Controller Area Network (CAN) control over the motors using an imbedded SimuLink Model.

3.4 EV Test Bed Software

The Opal-RT unit is run by RT-LAB, which utilizes MATLAB's Simulink to send control commands via CAN to the motors. The control layer in Simulink is shown in Figure 3-6.

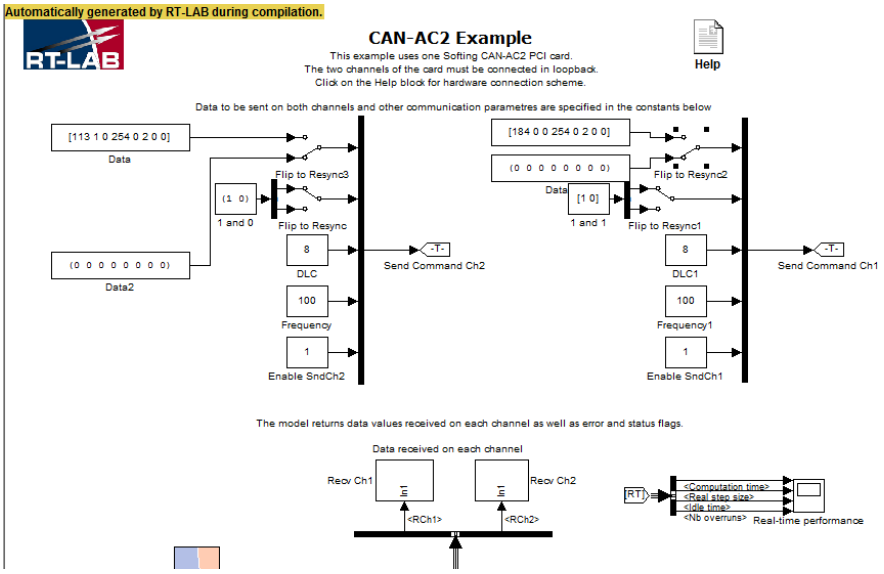

Figure 3-6: Simulink Model

The DMOC Controllers are configured using a program provided by Azure Dynamics called "CCShell". CCShell is used to modify DMOC calibration parameters as well as view and record real-time parameters. This software was utilized for data recording in this study. Figure 3-7 shows an example of user interface of CCShell. Serial connection to the motor drives allows for communication from PC to DMOC through CCShell.

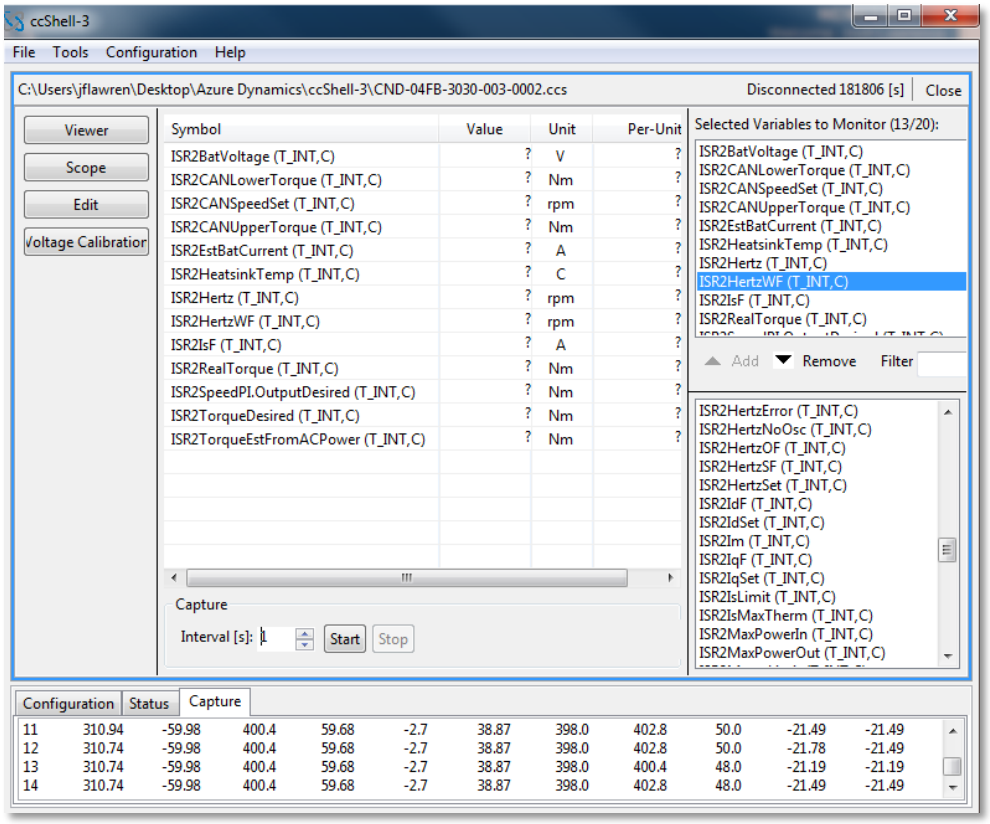

Figure 3-7: CCShell Interface

3.5 EV Test Bed Motor Control

The DMOC445 and DMOC645 controllers are DSP-controlled inverters used for controlling the AC55 and AC90 3-phase induction motors. A DMOC connection schematic is shown in Figure 3-8. Both controllers use a field oriented control algorithm and generate Space Vector PWM signals to feed gate signals to the inverter. Speed and position information is found using a 60-tooth quadrature encoder and is fed back to the DMOC [15,16]. Using the OPAL-RT HIL unit, torque or speed control for each motor can be implemented over the CAN network. The CAN application layer consists of a proportional-integral controller with output saturation and anti-windup.

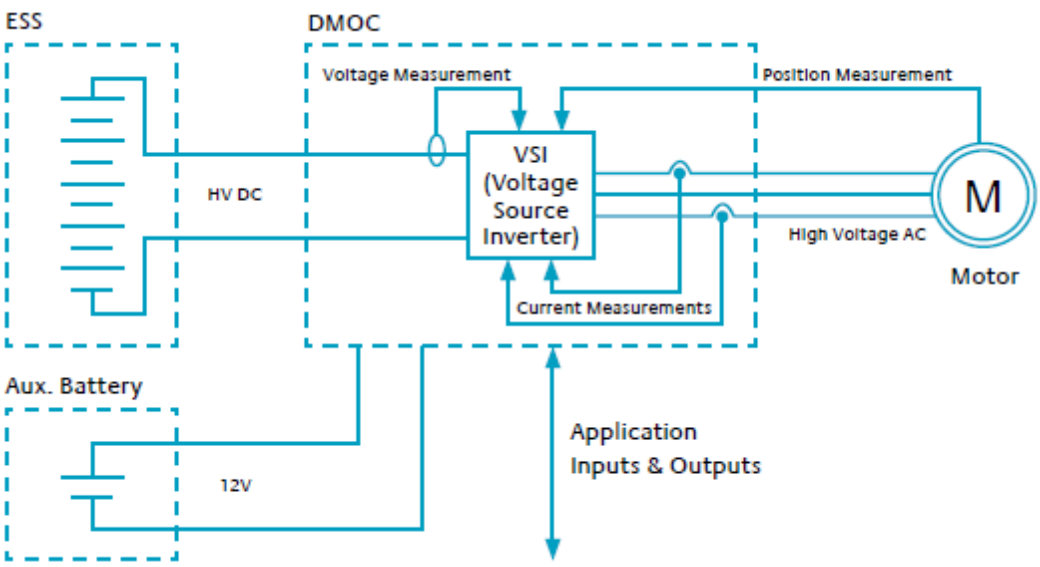

Figure 3-8: DMOC Control Schematic [15]

Using an 8-byte CAN command, each motor can either be set for speed control or torque control. This is dictated by the lower and upper torque limit values, as seen in Table 3-3. This table has been recreated from information found in *Azure Dynamics Can-Controlled Application User Manual* [17].

Table 3-3: Motor Control Mode

Condition	Controller Mode
LowerTorqueLimit<UpperTorqueLimit	Speed Control Mode
LowerTorqueLimit=UpperTorqueLimit	Torque Control Mode
LowerTorqueLimit>UpperTorqueLimit	Motor torque set to zero

All 16 bit signals in CAN messages use the signed Q10 format, so 1 per-unit equals 1024 and -1 per-unit equals -1024. Negative numbers use two's complement and all messages are little endian, least significant byte first. A CAN message byte string with each byte description is described below in Table 3-4.

Table 3-4: CAN Control Message

ID	Byte 0	Byte 1	Byte 2	Byte 3	Byte 4	Byte 5	Byte 6	Byte 7
	LSB	MSB	LSB	MSB	LSB	MSB	LSB	MSB
EEXCANCommandID	CANSpeedSet (1024 = 2500 rpm)		LowerTorqueLimit (1024 = 100 Nm)		UpperTorqueLimit (1024 = 100 Nm)		reserved for factory use VCU MUST SEND 0x00, 0x00 (ALL ZEROS)	

All input commands had to be converted into CAN messages from real values to send to the motors. Figure 3-9 lists the converted real speed and torque values into the correct CAN message.

Torque (N-m)	Can Message	
-100	0	252
-90	102	252
-80	205	252
-70	51	253
-60	154	253
-50	0	254
-40	102	254
-30	205	254
-20	51	255
-10	154	255
0	0	0
5	51	0
10	102	0
15	154	0
20	205	0
25	0	1
30	51	1
35	102	1
40	154	1
45	205	1
50	0	2
55	51	2
60	102	2
65	154	2
70	205	2
75	0	3
80	51	3
85	102	3
90	154	3
95	205	3
100	0	4

Speed (RPM)	Can Message	
0	0	0
50	20	0
100	41	0
150	61	0
200	82	0
250	102	0
300	123	0
350	143	0
400	164	0
450	184	0
500	205	0
550	225	0
600	246	0
650	10	1
700	31	1
750	51	1
800	72	1
850	92	1
900	113	1
950	133	1
1000	154	1
1050	174	1
1100	195	1
1150	215	1
1200	236	1
1250	0	2
1300	20	2
1350	41	2
1400	61	2
1450	82	2
1500	102	2
1550	123	2
1600	143	2
1650	164	2
1700	184	2
1750	205	2
1800	225	2
1850	246	2
1900	10	3
1950	31	3
2000	51	3

Figure 3-9: Torque and Speed Converted CAN Messages

Chapter 4

Experimental Setup

4.1 Introduction

To properly ensure validation of Pritchard's predictive analysis in the overrunning situation it was imperative to understand fully the workings of the torque converter and its integration into the transmission [3]. An Allison PTS-2500 Series transmission was completely disassembled in order to fully understand all components and how they interacted with the torque converter.

Figure 4-1: Disassembled Allison 2500 PTS Transmission

The turbine shaft was removed with the C1/C2 clutch pack. The turbine shaft is splined to align with the turbine inside the torque converter. It also has a larger spline that mates with the clutch pack

itself. The clutch pack was removed from the turbine shaft and the large spline was milled down to allow for coupling with the motor.

Figure 4-2: Removed Turbine Shaft

The stator shaft was then removed from the bell housing of the transmission and pressed out of the pump housing and pump cover assembly. Two ports for input and output fluid flow were welded onto the stator shaft allowing for an external pumping system to provide fluid to the torque converter.

Figure 4-3: Removed Stator Shaft

4.2: Fluid System

In normal in-vehicle operation, fluid flow through the transmission and torque converter is provided by a positive displacement pump, or gear pump. This pump is coupled to the engine and spins at engine speed; therefore, fluid flow rate is directly correlated to the speed at which the pump is spinning.

Electronically actuated solenoids controlled by the transmission control module (TCM) direct the fluid throughout the transmission and also the torque converter. The torque converter input flow fluid rate and direction are determined by the TCM, which dictates the engagement of the lock-up clutch inside the torque converter. The complexity of the fluid flow not only inside the torque converter but the transmission itself makes isolating and characterizing a single component in the transmission is a challenge.

A simple fluid displacement test was run to size the external pump used in the fluid system. A Plexiglas plate was bolted on top of the gear pump that rotates with the engine, shown in Figure 4-4.

Figure 4-4: Positive Displacement Pump Sizing Test

The pump was rotated ten times, pumping fluid into a graduated cylinder. This amount was then converted into the amount that would be displaced at operational speeds. Although simple in design, this allowed for proper approximation of the requirements needed by the external electric motor driven positive displacement pump.

The fluid system is comprised of a SHURflo electric motor driven positive displacement pump. The specifications are shown in Table 4-1.

Table 4-1: Positive Displacement Pump Specifications

SHURflo Electric Motor Driven Positive Displacement Pump		
Pump Speed	Rpm	1750
Motor Power	HP	330
Max Input Torque	in-lbs	45
Flow Rate (60 psi)	GPM	4
Motor Current	A	6.8

Society of Automotive Engineering's (SAE) Hydrodynamic Drive Test Code J643 was used as a reference for testing setup and procedure [18]. Fluid was supplied from a reservoir, with pressure regulators and dial gauges on the outlet of the pump and the outlet of the torque converter. This fluid system schematic is shown below in Figure 4-5.

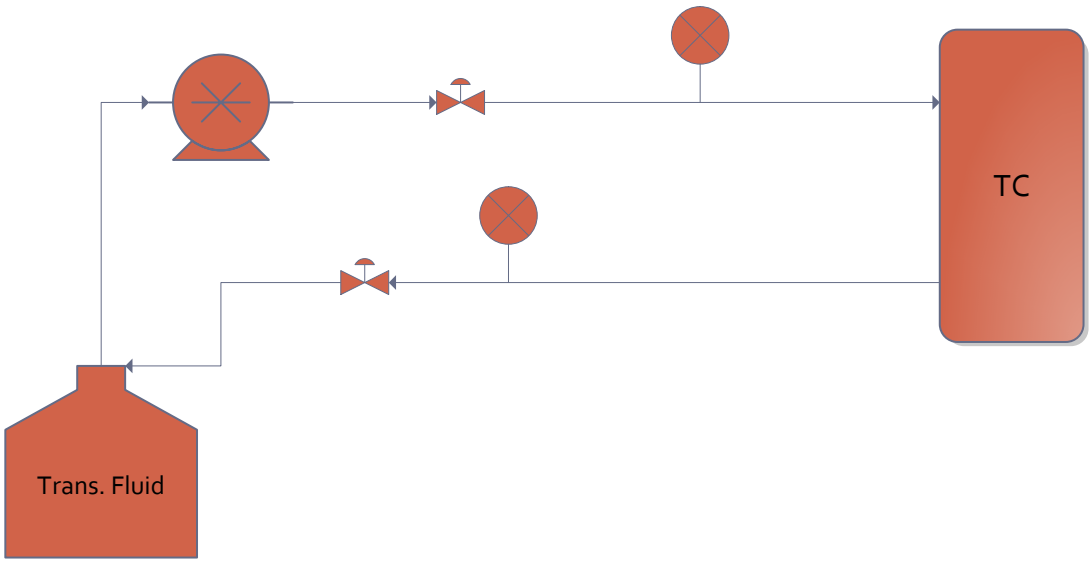

Figure 4-5: Fluid System Schematic

Thermocouples were used to measure ambient and outlet fluid temperatures and a Fluke Hydra Data Bucket was used for temperature recording. It was soon realized that the standard seals on the turbine and stator shaft did not completely seal the fluid, which caused improper flow and leaking. The seal closest to the outlet of the torque converter on the stator shaft was replaced as well as the seal at the end of the turbine shaft, which eliminated this issue. Flow direction was verified to ensure that the lock-up clutch would not engage.

4.3 Data Recording

As discussed in chapter three, each motor has a 60-tooth quadrature encoder for speed and position feedback. Torque was measured using current estimation from each of the motors. Using CCShell, a variety of parameters were recorded through the duration of the testing to yield the results seen in Chapter 5.

4.4 Experimental Testing

Tests were conducted at set impeller speeds of 400, 450, and 500 rpm with a varying range of turbine speeds to gather the experimental data. Operational range of the engine from idle to shift point is approximately 700 rpm to 1750 rpm. However, because of the mechanical dynamics of the torque converter and the control algorithm of the motors, instability in the system resulted at higher power demand situations. Because of this, testing was held to lower demand situations with the goal of capturing results that yielded similar trends compared to theoretical. Each test was run once the system stabilized for approximately thirty seconds and at each set impeller speed, turbine speed was varied by 50 RPM intervals. This was done from SR of approximately 0.1-2 with inlet pressure held constant at 60 psi and outlet pressure held constant at 15 psi. A test was conducted to see the influence of pressure on TR. An impeller speed of 400 RPM and turbine speed of 200

RPM was set and the test bed was run for approximately 30 seconds. One test used an inlet pressure of 40 PSI and an outlet pressure of 10 PSI, while the other used an inlet of 60 psi and outlet of 15 psi. The average SR and TR were taken as well as the percent difference of TR with the different pressures. As shown, there is 3.3% increase in TR with the higher pressure. Because of this, all testing was conducted at the higher set pressure.

Table 4-2: Low Pressure vs. High Pressure Test Results

	Average Speed Ratio	Average Torque Ratio
Low Pressure	0.5	1.24
High Pressure	0.5	1.27
Percent Difference		**3.30%**

A variable high voltage power supply provided a constant 310 VDC to the capacitor bank that fed the DMOC445 and DMOC645 motor drives. Two variable 12 VDC supplies were used to provide low voltage to the internal drive circuitry.

4.5 Experimental Calibration

Calibration of the experimental setup was necessary to determine the no load steady state losses caused by the bearings, friction and windage losses. This was characterized by driving only one electric motor and recording the required torque when providing a speed command. Once these values were collected, they were applied to the system to ensure the proper torque readings.

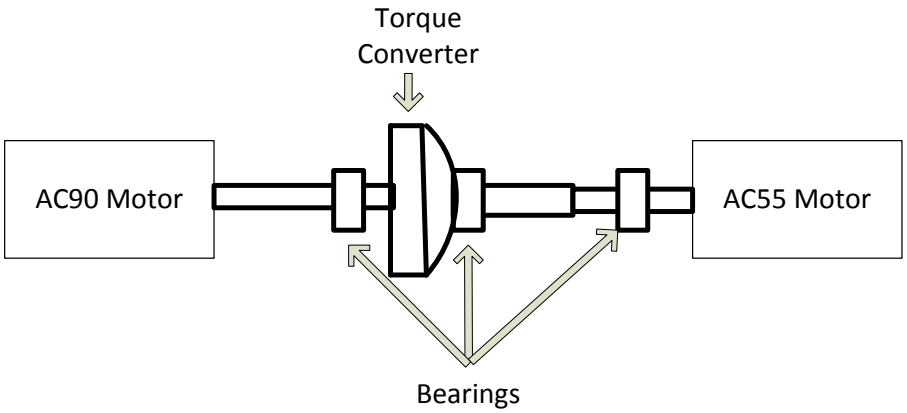

Figure 4-6: System Losses

As seen in Figure 4-6, there are three pillow block bearings supporting the torque converter and its components. Two are supporting the torque converter and the other is supporting the turbine shaft. The AC90 Motor drives the torque converter housing and the impeller. The AC55 motor drives the turbine shaft. In addition to the two supporting bearings, the AC90 motor has to overcome the torque converter housing and mounting plate windage losses. Because of this, the system losses are subtracted out of the torque measurement of the AC90 motor. As speed increases, so does the amount of torque required for steady state conditions as shown in Figure 4-7.

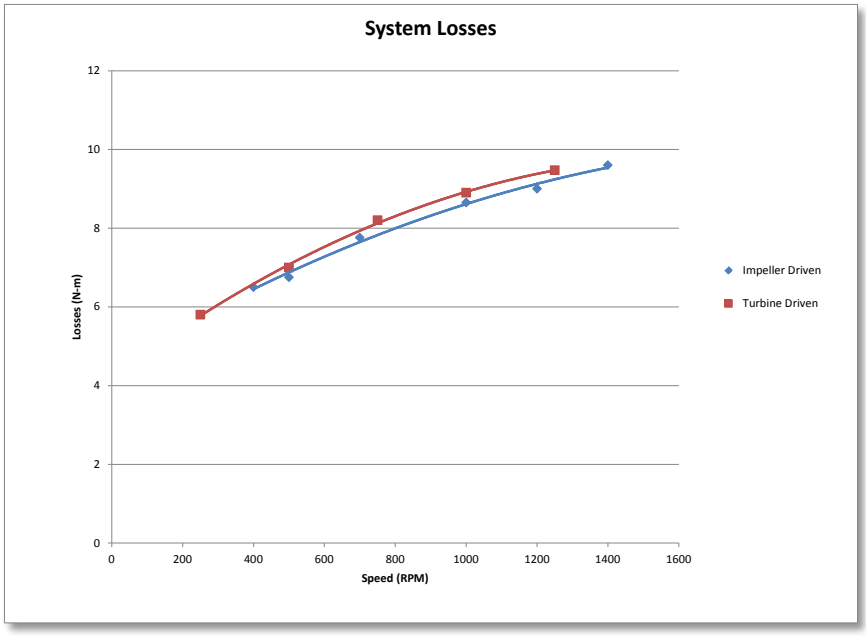

Figure 4-7: System Losses

This is assumed to be mainly windage losses from the torque converter and mounting plate. The slight discrepancy found between losses in the system when the turbine side is driven versus when the impeller side is driven can be accounted for in the torque converter. When the turbine side is driven it is essentially overrunning the torque converter until the impeller gets up to speed. The slippage occurring in that regime can account for the turbine driven test to have slightly higher losses.

Chapter 5

Results and Discussion

5.1 Introduction

Using the test setup described in Chapter 4, the following results were found and compared to those found in Pritchard's study as well as Kotwicki's. Although there were a variety of variables contributing to the yielded results, comparison and validation was still accomplished based on the results presented in the following section.

5.2 Comparative Analysis

The first comparison made was speed ratio vs. torque ratio. This is an industry standard plot for mapping torque converter operation and an excellent way to determine if the experimental results are in line with what is expected to happen over SR of zero to two. Comparing Pritchard's SR vs. TR curve to the experimental data, it is clear that the trend of torque multiplication occurs at SRs less than 0.9 and the TR goes to one at SRs greater than one.

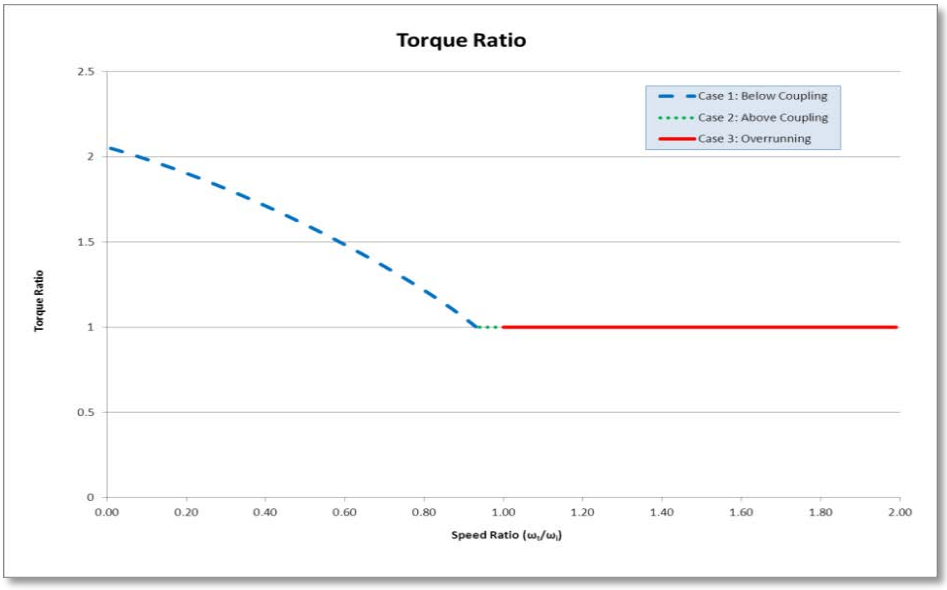

Figure 5-1: Theoretical SR vs. TR Curve

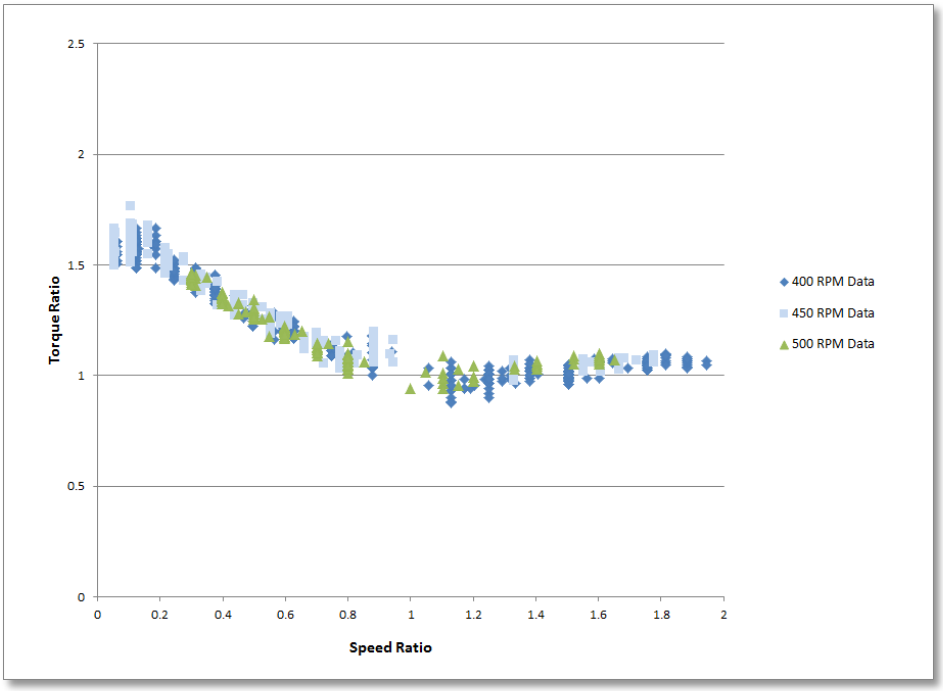

Figure 5-2: Experimental SR vs. TR Results

Although there is some discrepancy in the efficiency loss indicated by the experimental results to the optimized theoretical results this can be attributed to the lower operating range of the torque converter. It is expected that as impeller speed gets to higher power situations, the results would fit more closely with the theoretical curve. Additionally, the values used for Pritchard's predictive modeling found in Table 2-1 are approximations due to the difficulty of measuring them. At SR greater than one, it is clear that through all experimentation the TR is approximately one as is expected with any torque converter. This further validates the results found in this experiment.

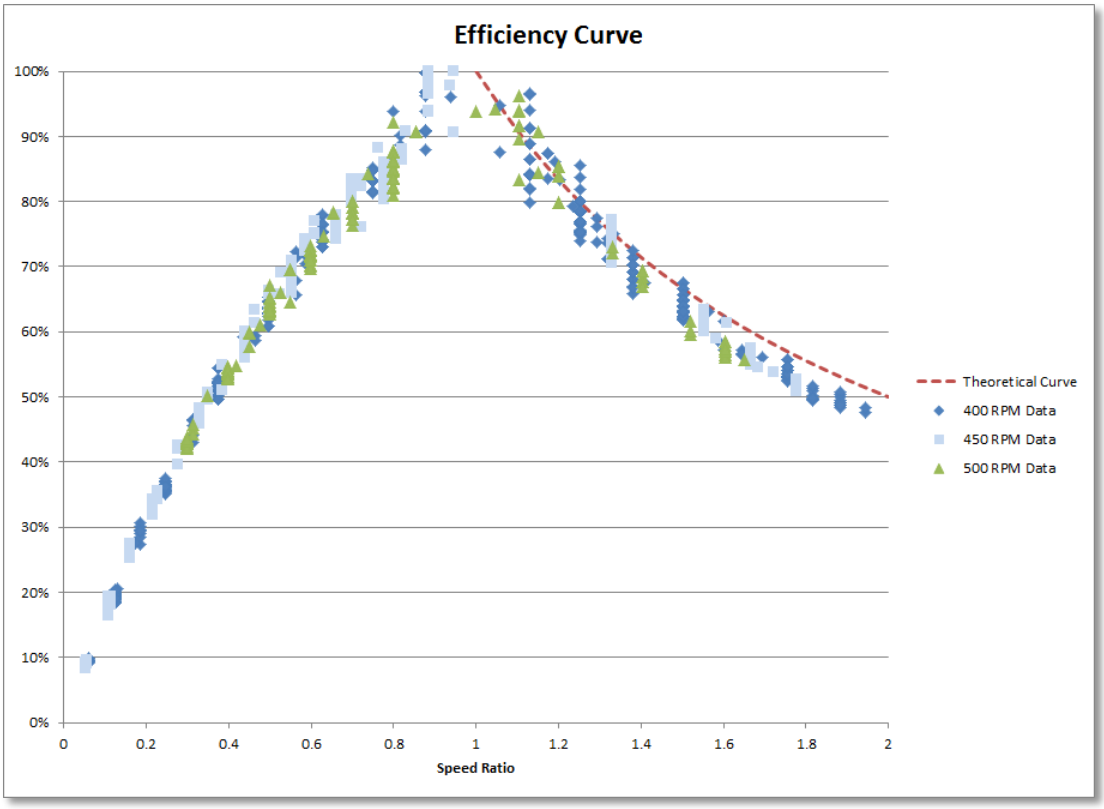

Figure 5-3: Torque Converter Efficiency Curve

Comparing the efficiency curve found from experimental data to the efficiency curves developed by Jandasek, it is clear that the torque converter is operating in a similar manner over a SR between zero and one. It is interesting to note the results found for SR greater than one. This again is expected and further validates the experimental results; as SR increases to two the efficiency should be approximately 50% because at SR greater than one the torque ratio is one. Figure 5-3 also shows the theoretical curve for SR greater than one. As indicated, the experimental data correlates directly with the theoretical curve.

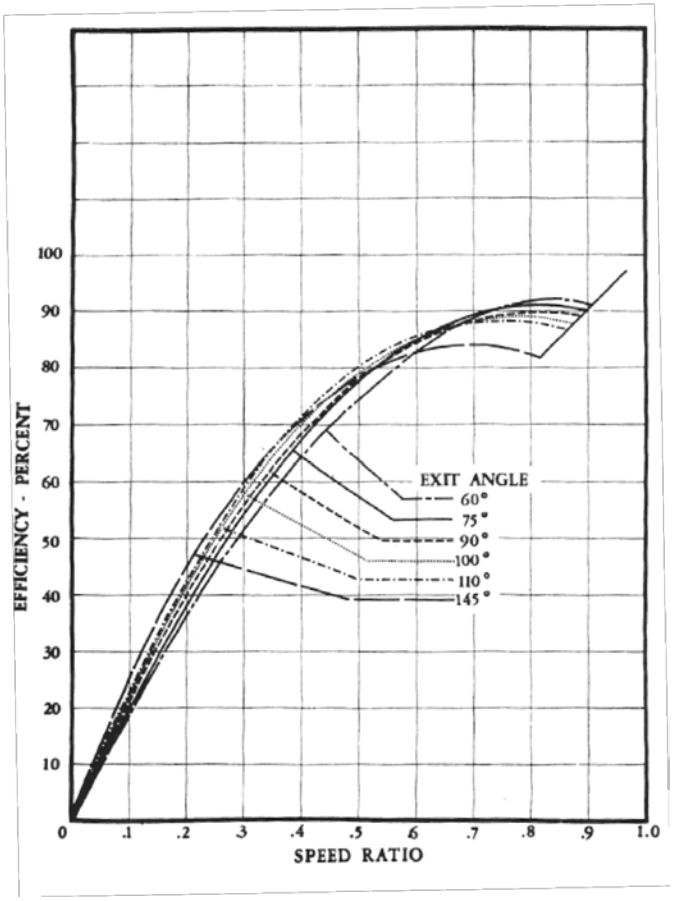

Figure 5-4: Theoretical Efficiency Curves from Jandesek [7]

Looking at SAE's Hydrodynamic test code J643, the efficiency curve again matches the experimental result. In above coupling regime, where SR is approximately 0.9-1.0, the logarithmic trend in both theoretical efficiency curves becomes linear. Although not as drastic, it can be seen in the experimental results to have a similar trend as that shown below in Figure 5-5.

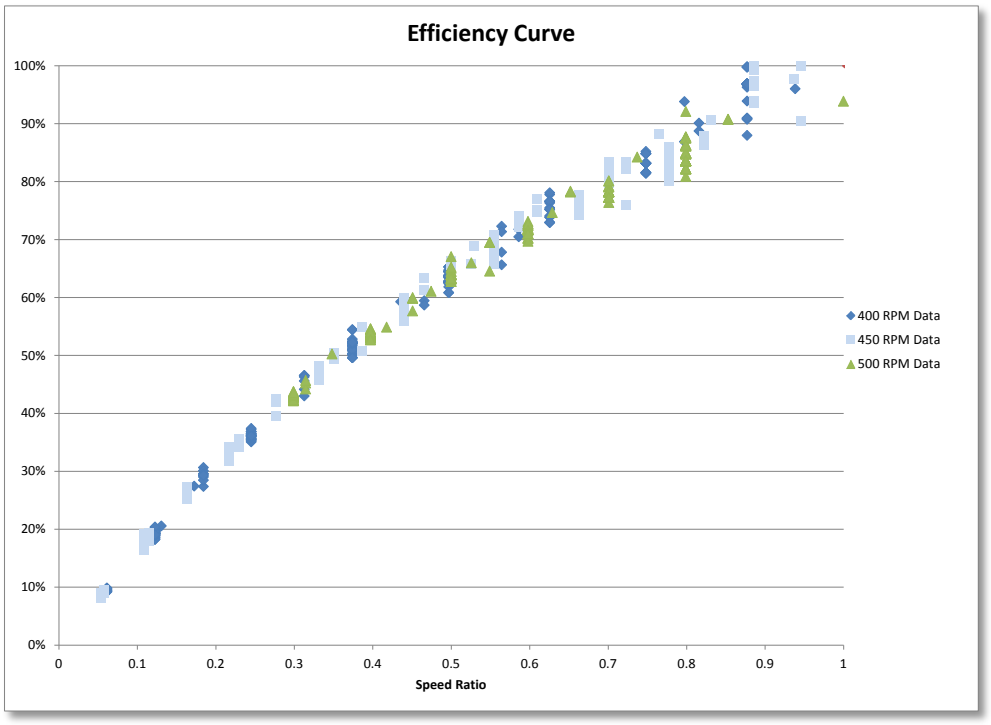

Figure 5-5: Experimental Efficiency Plot of SR from 0-1

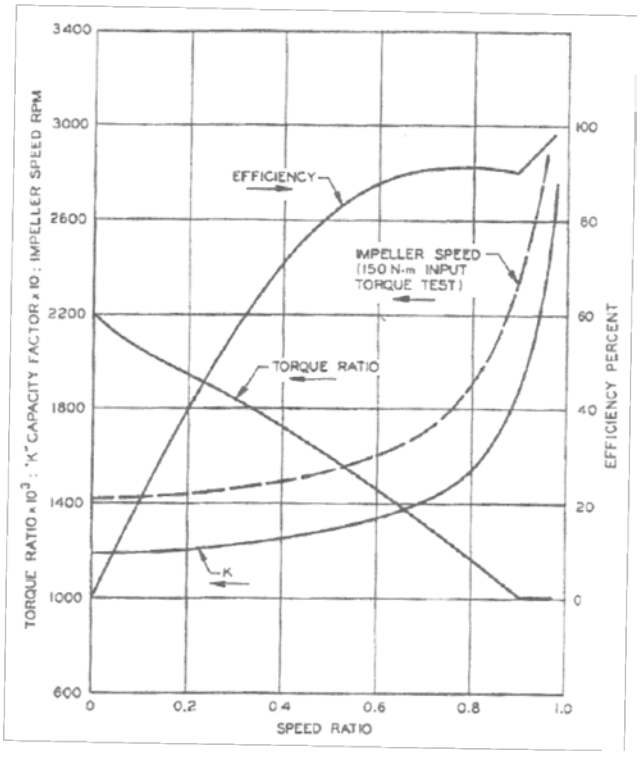

Figure 5-6: Typical Torque Converter Characteristics [18]

Figure 5-7 plots the SR vs. turbine torque divided by impeller speed squared of the experimental results. This graph clearly illustrates the same trend as seen in Figure 5-8, Pritchard's predictive modeling curve.

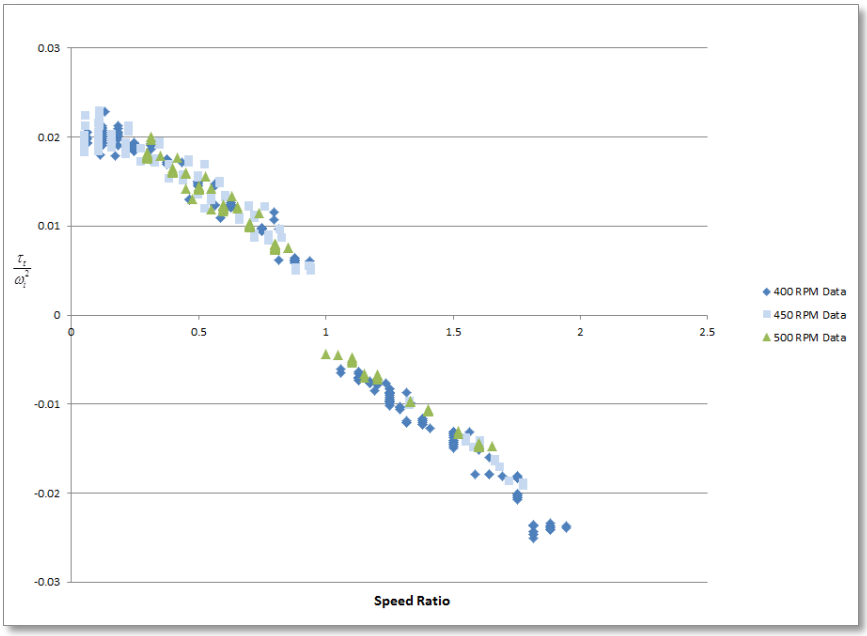

Figure 5-7: Turbine Torque Divided by Pump Speed Squared vs. SR

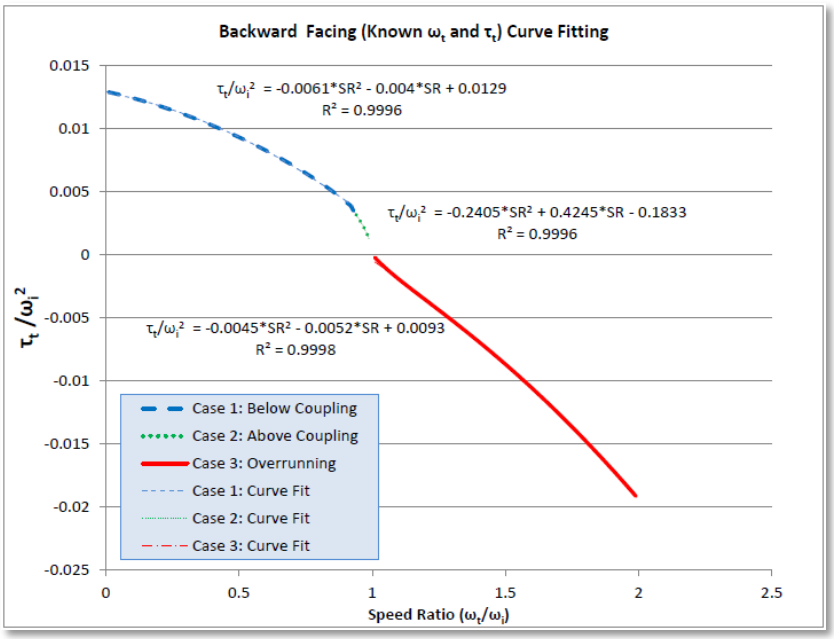

Figure 5-8: Predictive Model of Turbine Torque Divided by Impeller Speed Squared vs. SR[3]

This specific comparison is important because it shows that not only does the turbine torque become negative at SR greater than 1, but it infers that the volumetric flow rate, Q, does as well. This is valuable in supporting the predictive modeling done by Pritchard.

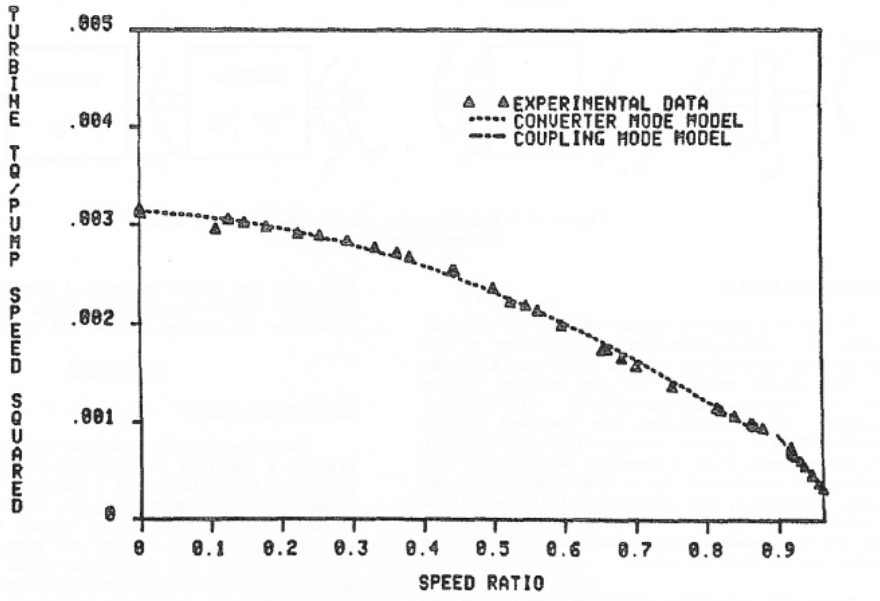

Figure 5-9: Kotwicki SR vs. Turbine Torque/Pump Speed Squared [11]

Figure 5-9 shows Kotwicki's curve of SR vs. turbine torque divided by pump speed squared further supports the experimental results found in this study, although Kotwicki does not explore the overrunning regime.

Chapter 6

Future Work

6.1 Extension of Experiments in this Study

An extension of this research would be to conduct the same experimental procedure at higher demand situations. This could yield even more conclusive results and would be an interesting comparison to how the converter operated during the experimental tests conducted in this study. Additionally, using torque transducers on either side of the torque converter would allow for an additional torque and speed measurement that could be compared to that found using CCShell. This would allow for a more exact measurement of torque acting directly on either side of the torque converter and motor losses would not be a factor.

6.2 Post Transmission Parallel Hybrid Drive Train Optimization

With Pritchard's predictive modeling for the overrunning regime validated, investigation should take place into how to solve this issue in every vehicle that has a post transmission parallel hybrid drive train. One idea would be to introduce a one-way clutch between the electric motor and transmission; however, this would require further investigation as to how it would work without the vehicle rolling backwards when not wanted by the driver. The implementation of a slipper clutch between the electric motor and transmission could also be investigated. They are often seen on motorcycles to lessen the effects of engine braking. When the rear wheel of the motorcycle spins faster than the engine, a slipper clutch is designed to partially disengage reducing the amount of torque placed on the engine. This would be an interesting mechanism to test to see its effectiveness

in preventing torque converter overrunning when a back torque is applied from the electric motor on the transmission.

Another investigation could be made into disengaging the turbine completely from the transmission during times when the transmission is spinning faster than the engine. LuK, a European drivetrain firm has developed a torque converter that has two internal clutches. One is used for lock-up with another that disengages the impeller completely from the engine. This reduces idle losses to almost zero, increases the dampening effect of the torque converter on the drivetrain and decreases overall drivetrain noise, vibration and harshness (NVH). Additionally, it allows for engine revs to increase before the impeller is engaged, decreasing vehicle lag. They claim fuel economy savings of up to 5% [19]. This same principle could be applied to the turbine side with an additional clutch to eliminate overrunning in vehicles that have a post transmission parallel hybrid architecture.

6.2.1 Magnetorheological Fluid Implementation

With the popularity of hybrid vehicles growing exponentially, exploration into the use of a different kind of fluid coupling between the engine and transmission could be explored. One example is the use of magnetorheological fluid or MR Fluid. MR fluid is already being applied to the transportation industry in vehicle suspension and fan clutches. MR fluid has the ability to drastically change its viscosity depending on the presence and magnitude of a magnetic field. MR fluid contains an oil that suspends iron particles on the micron scale. The fluid can go from a liquid to a solid in a few thousandths of a second when actuated by an electromagnet. This would allow for the engagement and disengagement of the coupling between the engine and transmission. However, this would bring up two issues that would need to be investigated: Is this economically feasible with the current market price of MR fluid and what would be the effects on drive train NVH? These both

could be potentially solved if a MR fluid coupling was placed between the engine and torque converter and the transmission and electric motor. This would allow for use of the torque converter and its ability to multiply torque at SR less than one, disengage the torque converter from the engine at idle, and disengage the electric motor from the transmission in situations where the transmission is spinning faster than the engine.

Chapter 7

Conclusion

This study aimed to validate the predictive modeling and losses of the TC-210 torque converter found in the PHESB. Due to the PHESB post transmission parallel hybrid architecture; there are situations where the electric motor is spinning faster than the engine causing the torque converter to operate in the overrunning regime. The internal torque converter losses in this regime are not accounted for in most vehicle modeling and simulation software packages. This study built on the work of Pritchard and the predictive equations developed to account for the extra losses in the overrunning regime. Through experimental testing it was concluded that the theoretical models developed by Pritchard were supported and therefore validated by the experimental results found in this study. Because of this, it was also concluded that by adding the additional internal torque converter losses in the overrunning regime the torque converter losses modeled over a specific drive cycle are 19 times higher than ADVISOR predicted using its own lookup tables.

References

[1]Pritchard, Ewan G. D. "Performance Modeling of Hybrid and Plug-in Hybrid School Buses using Advisor." MS Thesis North Carolina State University, 2004. Print.Raleigh: .

[2]Barghout, Jeff, and Staci Haggis. *Plug-in Hybrid Electric School Bus Project: 2010 Program Report*. Advanced Energy, 2010. Web.

[3]Pritchard, Ewan G. D. "Torque Converter Interactions in a Parallel Post Transmission Hybrid Driveline." Diss North Carolina State Univserity, 2010. Print.Raleigh, North Carolina: .

[4]---. "Torque Converter Interactions in a Post Transmission Parallel Hybrid Driveline". *Vehicle Power and Performance Conference. IEEE 2011.* September 6th, Chicago, IL. IEEE , 2011. Print.

[5]Navistar, Inc. "MAXXFORCE 7 Overview." 2012.Web. 6/11/11 <http://www.maxxforce.com/Application/pickup-and-suv/Engine/MaxxForce_7>.

[6]Zotov, B. N. "Basic Difference between Hydraulic Clutches and Hydraulic Torque Converters." *Chemical and Petroleum Engineering* 43 (2007)Print.

[7]Jandasek, V. J. "The Design of Single-Stage, Three Element Torque Converter." *Society of Automotive Engineers* (1961)Print.

[8]Avallone, E. A. *Marks' Standard Handbook for Mechanical Engineers*. 11th edition ed. New York: McGraw-Hill, 2007. Print.

[9]Ejiri, E. "Analysis of Flow in the Lock-Up Clutch of an Automotive Torque Converter." *JSME International Journal* Volume 49.1 (2006): 131. Print.

[10]Pohl, B. "Transient Torque Converter Performance, Testing, Simulation and Reverse Engineering." *SAE International* (2003)Print.

[11]Kotwicki, A. J. "Dynamic Models for Torque Converter Equipped Vehicles." *International Congress & Exposition* 820393 (1982)Print.

[12]Fox, R. W., and A. T. McDonald. *Introduction to Fluid Mechanics*. 4th Edition ed. John Wiley & Sons, Inc., 1992. Print.

[13]Ishihara, T., and R. I. Emori. "Torque Converter as a Vibration Damper and its Transient Characteristics." *Society of Automotive Engineers* 501 (1966)Print.

[14]Hrovat, D., and W. E. Tobler. "Bond Graph Modeling and Computer Simulation of Automotive Torque Converters." *Franklin Institute* 319 (1985): 93. Print.

[15]Ballal, S. "Flux and Torque Estimation in Direct Torque Controlled (DTC) Induction Motor Drive." Thesis North Carolina State University, 2010. Print.Raleigh: .

[16]Gonen, T. *Electrical Machines with MATLAB*. Second Edition ed. CRC Press, 2012. Print.

[17]Azure Dynamics. *CAN-Controlled Application User Manual for Azure Dynamics DMOC Motor Controller*. MAN-080003-001 Vol. Woburn, MA: Azure Dynamics Inc., 2009. Print.

[18]*Surface Vehicle Recommended Practice*. (R) Hydrodynamic Drive Test Code ed. J643 Vol. Warrendale, PA: SAE International, 2011. Print.

[19]"Torque Converter Cuts Low RPM Diesel Losses." *Automotive Engineer* March, 2008 2008: 40. Print.